Parameterization of Cirrus Cloud Formation in Large Scale Models: Homogeneous Nucleation.

Donifan Barahona[1] and Athanasios Nenes[1,2*]

[1]School of Chemical and Biomolecular Engineering, Georgia Institute of Technology

[2]School of Earth and Atmospheric Sciences, Georgia Institute of Technology

311 Ferst Dr., Atlanta, GA, 30332, USA

*Corresponding author

Abstract

This work presents a new physically-based parameterization of cirrus cloud formation for use in large scale models which is robust, computationally efficient, and links chemical effects (e.g., water activity and water vapor deposition effects) with ice formation via homogenous freezing. The parameterization formulation is based on ascending parcel theory, and provides expressions for the ice crystal size distribution and the crystal number concentration, explicitly considering the effects of aerosol size and number, updraft velocity, and deposition coefficient. The parameterization is evaluated against a detailed numerical cirrus cloud parcel model (also developed during this study) where the solution of equations is obtained using a novel Lagrangian particle tracking scheme. Over a broad range of cirrus forming conditions, the parameterization reproduces the results of the parcel model within a factor of two and with an average relative error of -15%. If numerical model simulations are used to constraint the parameterization, error further decreases to 1 ± 28%.

1 Introduction

The effect of aerosols on clouds and climate is one of the major uncertainties in anthropogenic climate change assessment and prediction [*IPCC*, 2007]. Cirrus are of the most poorly understood systems, yet they can strongly impact climate. Cirrus are thought to have a net warming effect because of their low emission temperatures and small thickness [*Liou*, 1986]. They also play a role in regulating the ocean temperature [*Ramanathan and Collins*, 1991] and maintaining the water vapor budget of the upper troposphere and lower stratosphere [*Hartmann, et al.*, 2001]. Concerns have been raised on the effect of aircraft emissions [*Penner, et al.*, 1999; *Minnis*, 2004; *Stuber, et al.*, 2006; *IPCC*, 2007] and long-range transport of pollution [*Fridlind, et al.*, 2004] changing the properties of upper tropospheric clouds, i.e., cirrus and anvils, placing this type of clouds in the potentially warming components of the climate system.

Cirrus clouds form by the homogenous freezing of liquid droplets, by heterogeneous nucleation of ice on ice nuclei, and the subsequent grow of ice crystals [*Pruppacher and Klett*, 1997]. This process is influenced by the physicochemical properties of the aerosol particles (i.e., size distribution, composition, water solubility, surface tension, shape), as well as by the thermodynamical state (i.e., relative humidity, pressure, temperature) of their surroundings. Dynamic variability (i.e., fluctuations in updraft velocity) also impact the formation of cirrus clouds potentially enhancing the concentration of small crystals [*Lin, et al.*, 1998; *Kärcher and Ström*, 2003; *Hoyle, et al.*, 2005].

68 The potential competition between homogeneous and heterogeneous mechanisms has an
69 important impact on cirrus properties. For instance, by enhancing ice formation at low
70 relative humidity, heterogeneous effects may suppress homogeneous freezing and
71 decrease the ice crystal concentration of the newly formed cloud [*DeMott, et al.*, 1994;
72 *Kärcher and Lohmann*, 2002a; *Gierens*, 2003; *Haag, et al.*, 2003b]. It has been suggested
73 that heterogeneous freezing has an stronger impact on cirrus formation over polluted
74 areas [*Chen, et al.*, 2000; *Haag, et al.*, 2003b; *Abbatt, et al.*, 2006], at low updraft
75 velocities (less than 10 cm s^{-1}) [*DeMott, et al.*, 1997; *DeMott, et al.*, 1998; *Kärcher and*
76 *Lohmann*, 2003], and at temperatures higher than -38 °C where homogenous nucleation
77 is not probable [*Pruppacher and Klett*, 1997; *DeMott, et al.*, 2003]. On the other hand,
78 homogenous freezing is thought to be the prime mechanism of cirrus formation in
79 unpolluted areas, high altitudes, and low temperatures [*Heymsfield and Sabin*, 1989;
80 *Jensen, et al.*, 1994; *Lin, et al.*, 2002; *Haag, et al.*, 2003b; *Cantrell and Heymsfield*, 2005;
81 *Khvorostyanov, et al.*, 2006].
82
83 A major challenge in the description of cirrus formation is the calculation of the
84 nucleation rate coefficient, *J,* i.e., the rate of generation of ice germs per unit of volume.
85 Historically this has been accomplished through classical nucleation theory [*DeMott, et*
86 *al.*, 1997; *Pruppacher and Klett*, 1997; *Tabazadeh, et al.*, 1997], or using empirical
87 correlations [i.e., *Koop, et al.*, 2000]. The former requires the accurate knowledge of
88 thermodynamic properties, such as surface and interfacial tensions, densities, and
89 activation energies [*Cantrell and Heymsfield*, 2005]. With appropriate extensions [i.e.,
90 *DeMott, et al.*, 1994; *DeMott, et al.*, 1997; *Chen, et al.*, 2000; *Lin, et al.*, 2002], theory

91 included in cirrus formation simulations shows agreement with experimental
92 measurements and field campaigns [i.e., *Chen, et al.*, 2000; *Archuleta, et al.*, 2005;
93 *Khvorostyanov, et al.*, 2006]. Still, there is much to learn on the physical properties of
94 aqueous solutions and ice at low temperatures. Until now, the most reliable methods to
95 calculate J are based on laboratory measurements [*Lin, et al.*, 2002]. *Koop et al.* [2000]
96 used experimental data to develop a parameterization showing J as a function of water
97 activity and temperature (rather than on the nature of the solute), which has been
98 supported by independent measurements of composition and nucleation rate during field
99 campaigns and cloud chamber experiments [i.e., *Haag, et al.*, 2003a; *Möhler, et al.*,
100 2003].
101
102 The formation of cirrus clouds is realized by solving the mass and energy balances in an
103 ascending (cooling) cloud parcel [e.g., *Pruppacher and Klett*, 1997]. Although models
104 solve the same equations (described in section 2.1), assumptions about aerosol size and
105 composition, J calculation, deposition coefficient, and numerical integration procedure
106 strongly impact simulations. This was illustrated during the phase I of the Cirrus Parcel
107 Model Comparison Project [*Lin, et al.*, 2002]; for identical initial conditions, seven state-
108 of-the-art models showed variations in the calculation of ice crystal concentration, N_c,
109 (for pure homogeneous freezing cases) up to a factor of 25, which translates to a factor of
110 two difference in the infrared absorption coefficient. *Monier, et al.* [2006] showed that a
111 three order of magnitude difference in the calculation of J , which is typical among
112 models at temperatures above -45 °C, will account only for about a factor of two
113 variation in N_c calculation. The remaining variability in N_c results from the numerical

114 scheme used in the integration, the calculation of the water activity inside the liquid
115 droplets at the moment of freezing, and the value of the water vapor deposition
116 coefficient.
117
118 Introducing ice formation microphysics in large scale simulations requires a physically-
119 based link between the ice crystal size distribution, and the precursor aerosol and
120 thermodynamic state. Empirical correlations derived from observations are available [i.e.,
121 *Koenig*, 1972]; their validity however for the whole spectra of cirrus formation
122 conditions present in a GCM is not guaranteed. Numerical simulations have been used to
123 produce prognostic parameterizations for cirrus formation [*Sassen and Benson*, 2000; *Liu*
124 *and Penner*, 2005], which relate N_c to updraft velocity and temperature (the *Liu and*
125 *Penner* parameterization also takes into account the dependency of N_c on the precursor
126 aerosol concentration, and was recently incorporated into the NCAR Community
127 Atmospheric Model (CAM3) [*Liu, et al.*, 2007]). Although theoretically based, these
128 parameterizations are constrained to a particular set of parameters (i.e., deposition
129 coefficient, aerosol composition and characteristics) used during the model simulations,
130 the value of which is still uncertain. *Kärcher and Lohmann* [2002b; 2002a] introduced a
131 physically-based parameterization solving analytically the parcel model equations. In
132 their approach a "freezing time scale" is defined, related to the cooling rate of the parcel,
133 and used to approximate the crystal size distribution at the peak saturation ratio through a
134 function describing the temporal shape of the freezing pulse. This function, along with
135 the freezing time scale, should be prescribed (also, the freezing pulse shape and freezing
136 time scale may still change with the composition and size of the aerosol particles). An

137 analytical fit of the freezing time scale based on *Koop et al.* [2000] data was provided by
138 *Ren and Mackenzie* [2005]. *Kärcher and Lohmann* parameterization have been applied
139 in GCM simulations [*Lohmann and Kärcher*, 2002] and extended to include
140 heterogeneous nucleation and multiple particle types [*Kärcher, et al.*, 2006]. All
141 parameterizations developed to date provide limited information on the ice crystal size
142 distribution, which is required for computing the radiative properties of cirrus clouds
143 [*Liou*, 1986].
144
145 In this work, we develop a new physically-based parameterization for ice formation from
146 homogeneous freezing in which we relax the requirement of prescribed parameters. The
147 parameterization unravels much of the stochastic nature of the cirrus formation process
148 by linking crystal size with the freezing probability, and explicitly considers the effects
149 the deposition coefficient and aerosol size and number, on N_c. With this approach, the
150 size distribution, peak saturation ratio, and ice crystal concentration can be computed.
151 The parameterization is then evaluated against a detailed numerical parcel model (also
152 presented here), which solves the model equations using a novel Lagrangian particle
153 tracking scheme.
154

155 ## 2 Numerical Cirrus Parcel Model

156 Homogenous freezing of liquid aerosol droplets is a stochastic process resulting from
157 spontaneous fluctuations of temperature and density within the supercooled liquid phase
158 [*Pruppacher and Klett*, 1997]. Therefore, only the fraction of frozen particles at some
159 time can be computed (rather than the exact moment of freezing). At anytime during the

160 freezing process, particles of all sizes have a finite probability of freezing; this implies
161 that droplets of the same size and composition will freeze at different times, so even
162 freezing of a perfectly monodisperse droplet population will result in a polydisperse
163 crystal population. This conceptual model can be extended to a polydisperse droplet
164 population; each aerosol precursor "class" will then form an ice crystal distribution with
165 its own composition and characteristics, which if superimposed, will represent the overall
166 ice distribution. In this section the formulation of a detailed numerical model, taking into
167 account these considerations, is presented. The equations of the model share similar
168 characteristics with those proposed by many authors [*Pruppacher and Klett*, 1997; *Lin, et*
169 *al.*, 2002, and references therein] as the ascending parcel framework is used for their
170 development.
171

172 **2.1 Formulation of Equations**

173 The equations that describe the evolution of ice saturation ratio, S_i (defined as the ratio of
174 water vapor pressured to equilibrium vapor pressure over ice), and temperature, T, in an
175 adiabatic parcel, with no initial liquid water present, are [*Pruppacher and Klett*, 1997].

176
$$\frac{dS_i}{dt} = -\frac{M_a p}{M_w p_i^o}\frac{dw_i}{dt} - (1+S_i)\left[\frac{\Delta H_s M_w}{RT^2}\frac{dT}{dt} - \frac{gM_a}{RT}V\right] \quad (1)$$

177
$$\frac{dT}{dt} = -\frac{gV}{c_p} - \frac{\Delta H_s}{c_p}\frac{dw_i}{dt} \quad (2)$$

178 where ΔH_s is the latent heat of sublimation of water, g is the acceleration of gravity, c_p is
179 the heat capacity of air, p_i^o is the ice saturation vapor pressure at T [*Murphy and Koop,*
180 2005], p is the ambient pressure, V is the updraft velocity, M_w and M_a are the molar
181 masses of water and air, respectively, and R is the universal gas constant. For simplicity,

182 radiative cooling effects have been neglected in equation (2), although in principle they
183 can be readily included. By definition, the ice mixing ratio in the parcel, w_i, is given by

184 $$w_i = \frac{\rho_i}{\rho_a}\frac{\pi}{6}\int_{D_{o,\min}}^{D_{o,\max}}\int_{D_{c,\min}}^{D_{c,\max}} D_c^3 n_c(D_c, D_o) dD_c dD_o \quad (3)$$

185 where ρ_i and ρ_a are the ice and air densities, respectively. D_c is the volume-equivalent
186 diameter of an ice particle (assuming spherical shape), D_o is the wet diameter of the
187 freezing liquid aerosol, $n_c(D_c, D_o) = \frac{dN_c(D_o)}{dD_c}$ is the ice crystal number distribution
188 function, $N_c(D_o)$ is the number density of ice crystals in the parcel formed at D_o; $D_{o,min}$,
189 and $D_{o,max}$ limit the liquid aerosol size distribution, and $D_{c,min}$ and $D_{c,max}$ the ice crystal
190 size distribution. Taking the time derivative of (3) we obtain

191 $$\frac{dw_i}{dt} = \frac{\rho_i}{\rho_a}\frac{\pi}{2}\int_{D_{o,\min}}^{D_{o,\max}}\int_{D_{c,\min}}^{D_{c,\max}} D_c^2 \frac{dD_c}{dt} n_c(D_c, D_o) dD_c dD_o \quad (4)$$

192 where the term $D_c^3 \frac{\partial n_c(D_c, D_o)}{\partial t}$ was neglected as instantaneous nucleation does not
193 contribute substantially to the depletion of water vapor in the cloudy parcel. The growth
194 term in equation (4) is given by [*Pruppacher and Klett*, 1997]

195 $$\frac{dD_c}{dt} = \frac{(S_i - S_{i,eq})}{\Gamma_1 D_c + \Gamma_2} \quad (5)$$

196 with

197 $$\Gamma_1 = \frac{\rho_i RT}{4 p_i^o D_v M_w} + \frac{\Delta H_s \rho_i}{4 k_a T}\left(\frac{\Delta H_s M_w}{RT} - 1\right) \qquad \Gamma_2 = \frac{\rho_i RT}{2 p_i^o M_w}\sqrt{\frac{2\pi M_w}{RT}}\frac{1}{\alpha_d} \quad (6)$$

where k_a is the thermal conductivity of air, D_v is the water vapor diffusion coefficient from the gas to ice phase, $S_{i,eq}$ is the equilibrium ice saturation ratio, and α_d is the water vapor deposition coefficient.

The crystal size distribution, $n_c(D_c, D_o)$ is calculated by solving the condensation equation [*Seinfeld and Pandis*, 1998]

$$\frac{\partial n_c(D_c, D_o)}{\partial t} = -\frac{\partial}{\partial D_c}\left(n_c(D_c, D_o)\frac{dD_c}{dt} \right) \tag{7}$$

subject to the boundary and initial conditions (neglecting any change of volume upon freezing),

$$\left.\frac{\partial n_c(D_c, t)}{\partial t}\right|_{D_c = D_o} = n_o(D_o, t)\frac{\partial P_f(D_o, t)}{\partial t} \equiv \psi(D_o, t) \quad ; \quad n_c(D_c, D_o, 0) = 0 \tag{8}$$

where $n_o(D_o, t)$ is the liquid aerosol size distribution function, $\psi(D_o, t)$ is the nucleation function which describes the number concentration of droplets frozen per unit of time, and $P_f(D_o, t)$ is the cumulative probability of freezing, given by [*Pruppacher and Klett*, 1997]

$$P_f(D_o, t) = 1 - \exp\left(-\frac{\pi}{6}\int_0^t D_o^3 J(t) dt \right) \tag{9}$$

and

$$\frac{\partial P_f(D_o, t)}{\partial t} = \frac{\pi}{6} D_o^3 J(t) \exp\left(-\frac{\pi}{6}\int_0^t D_o^3 J(t) dt \right) \tag{10}$$

$J(t)$ is the homogeneous nucleation rate coefficient, and describes the number of ice germs formed per unit of volume of liquid droplets per unit of time [*Pruppacher and Klett*, 1997].

218

219 Equation (7) is a simplified version of the continuous general dynamic equation for the
220 ice crystal population [*Gelbard and Seinfeld*, 1980; *Seinfeld and Pandis*, 1998], where
221 the nucleation term has been set as a boundary condition to facilitate its solution. This can
222 be done since the size of the ice particles equals the size of the precursor aerosol only at
223 the moment of freezing.

224

225 The evolution of the liquid droplets size distribution, $n_o(D_o,t)$, is calculated using an
226 equation similar to (7),

227 $$\frac{\partial n_o(D_o,t)}{\partial t} = -\frac{\partial}{\partial D_o}\left(n_o(D_o)\frac{dD_o}{dt}\right) - \psi(D_o,t) \qquad (11)$$

228 The first term of the right hand side of equation (11) represents the growth of aerosol
229 liquid particles by condensation of water vapor, and the second term the removal of
230 liquid particles by freezing. Boundary and initial conditions for (11) are simply the initial
231 aerosol size distribution and the condition of no particles at zero diameter.

232

233 **2.2 Numerical Solution of parcel model equations**

234 Equations (1) to (11) are solved numerically using a Lagrangian particle tracking scheme;
235 this uses a particle tracking grid for the ice crystal population (the growth of groups of ice
236 crystals is followed after freezing) coupled to a moving grid scheme (the liquid aerosol
237 population is divided into bins the size of which is changing with time), for the liquid
238 aerosol population (Figure 1). At any $t = t'$, the number of frozen aerosol particles is
239 calculated using (9) and placed in a node of the particle tracking grid, in which their
240 growth is followed. This group of ice crystals represents a particular solution of (7) for

241 the case in which all particles freeze at the same time and have the same size and
242 composition. Since a particular solution of (7) can be obtained for each time step and
243 droplet size, then the general solution of (7) is given by the superposition of all generated
244 ice crystal populations during the freezing process; w_i can then be calculated and
245 equations (1-4) readily solved. To describe the evolution of $n_o(D_o,t)$, a moving grid is
246 employed, where frozen particles are removed from each size bin (which is in turn
247 updated to its equilibrium size) after each time step.
248
249 Since all ice particles are allowed to grow to their exact sizes, the effect of numerical
250 diffusion is small. The discretization of (7) transforms the partial differential equation
251 into a system of ordinary differential equations, each of which represents the growth of a
252 monodisperse ice crystal population. Thus, an Euler integration scheme can be used
253 without substantial losses in accuracy. This is at expense of setting a large grid: the total
254 number of nodes in the particle tracking grid is the product of the number of time steps
255 by the number of nodes of the liquid aerosol moving grid. The particle tracking grid size
256 can be substantially reduced by grouping the newly frozen particles in a fewer number of
257 sizes [i.e., *Khvorostyanov and Curry*, 2005],

258 $$\left.\frac{\partial n_c(D_c,\overline{D}_o',t)}{\partial t}\right|_{D_c=D_o'} = \frac{1}{D_{upper}-D_{lower}}\int_{D_{lower}}^{D_{upper}} n_o(D_o,t)\frac{\partial P_f(D_o,t)}{\partial t}\,dD_o \qquad (12)$$

259 where $\overline{D}_o'$ is the assumed size of the frozen particles. If all aerosol particles freeze at the
260 same size, the integral in (12) is evaluated over the entire size spectrum of the liquid
261 aerosol population. A further reduction in the size of the particle tracking grid is achieved
262 by recognizing that the freezing process occurs after some threshold S_i is reached [*Sassen*

263 *and Benson*, 2000; *Kärcher and Lohmann*, 2002b]; therefore the initial time step is set to
264 $2V^{-1}$ s, and reduced to $0.05V^{-1}$ s (with V in m s^{-1}) when the nucleation event starts ($J > 10^4$
265 $m^{-3}s^{-1}$), only after which the growth of ice particles is accounted for.
266
267 **2.3 Baseline simulations**
268 The formulation of the parcel model was tested using the baseline protocols of *Lin et al.*
269 [2002]. Pure ice bulk properties were used to calculate the growth terms (equations 5-6).
270 D_o was assumed as the equilibrium size at S_i, given by Köhler theory [*Pruppacher and*
271 *Klett*, 1997], and solved iteratively using reported bulk density and surface tension data
272 [*Tabazadeh and Jensen*, 1997; *Myhre, et al.*, 1998]. This assumption may bias the results
273 of the parcel model simulations at low T and high V [*Lin, et al.*, 2002]; alternatively the
274 aerosol size can be calculated using explicit growth kinetics for which the water vapor
275 uptake coefficient from the vapor to the liquid phase is uncertain [*Lin, et al.*, 2002]
276 (recent measurements indicate a value between 0.4 and 0.7 [*Gershenzon, et al.*, 2004]). J
277 was calculated using the *Koop et al*. [2000] parameterization due to its simplicity and its
278 widely accepted accuracy for a broad range of atmospheric conditions [i.e., *Abbatt, et al.*,
279 2006] (in principle any model for J can be used.) The dry aerosol population was
280 assumed to be pure H_2SO_4, lognormally distributed with geometric mean diameter, $D_{g,\,dry}$
281 = 40 nm, geometric dispersion, $\sigma_{g,\,dry}$ = 2.3, and total number concentration, N_o = 200 cm^{-3}.
282 The runs were performed using 20 size-bins for the liquid aerosol; the newly frozen
283 particles were grouped into 4 size classes, producing a grid between 1500 and 2000
284 nodes; numerical results showed that little accuracy was gained by using a finer grid (not

285 shown). Runs of the parcel model using a regular PC (2.2 GHz processor speed and 1 GB
286 of RAM), usually took between 5 and 12 min.
287
288 Figure 2 shows results of the performed simulations for the protocols of *Lin, et al.* [2002]
289 and $\alpha_d = 1$, these simulations are intended to provide a common basis for comparison
290 with other models.. The value of α_d is still uncertain and may impact N_c [*Lin, et al.*,
291 2002]. Simulations using $\alpha_d = 0.1$ (not shown) produced N_c (cm^{-3}) of 0.20, 2.87, 24.06,
292 for the cases Ch004, Ch020 and Ch100, respectively, and 0.043, 0.535, and 5.98 for the
293 cases Wh004, Wh020 and Wh100, respectively. Results from the INCA campaign
294 summarized by *Gayet, et al.* [2004] indicate N_c around 1.71 cm^{-3} for T between -43 and -
295 53 °C, and N_c around 0.78 cm^{-3} for T between -53 and -63 °C with V mainly below 1 m
296 s^{-1}, at formation conditions consistent with a homogeneous nucleation mechanism [*Haag,*
297 *et al.*, 2003b]. These values are consistent with a low value for α_d (around 0.1) which is
298 supported by independent studies [*Gierens, et al.*, 2003; *Hoyle, et al.*, 2005;
299 *Khvorostyanov, et al.*, 2006; *Monier, et al.*, 2006]. However, direct comparison of the
300 parcel model with experimental results may presuppose a rather simplistic view of the
301 cirrus formation process, and overlook other effects (i.e., variation in aerosol
302 characteristics, V and T fluctuations [*Kärcher and Ström*, 2003; *Kärcher and Koop*,
303 2005]). Theoretical calculations and direct experimental observations have reported α_d
304 values from 0.03 to 1 at temperatures within the range 20 to 263 K [i.e., *Haynes, et al.*,
305 1992; *Wood, et al.*, 2001]. Due to these considerations α_d is considered in this work a
306 highly uncertain parameter for which more study is required.
307

3 Parameterization of Ice Nucleation and Growth

3.1 Parameterization of $n_c(D_c, D_o)$

The ultimate goal of this study is to develop an approximate analytical solution of equations (5-12) to predict number and size of ice crystals as a function of cloud formation conditions. For this, a link should be established between ice particle size and their probability of freezing at the time of nucleation; such link defines $n_c(D_c, D_o)$ at each time during the freezing pulse. $n_c(D_c, D_o)$ is determined for a given S_i profile by tracing back the growth of a group of ice crystals particles of size D_c down to D_o (Figure 3). In the following derivation we assume that most of the crystals are nucleated before maximum saturation ratio, $S_{i,max}$, is reached. The implications of this assumption are discussed in section 4. We start by writing a solution of equation (7) in the form

$$n_c(D_c, D_o) = -\overline{n}_o(D_o)\frac{\partial P_f(S_o^{'})}{\partial D_c} \tag{13}$$

where $S_o^{'}$ is a value of $S_i < S_{i,max}$ at which the ice crystals were formed and $P_f(S_o^{'})$ represents the current fraction of crystals of size D_c, that come from liquid aerosol particles of size D_o. $\overline{n}_o(D_o)$ is the average $n_o(D_o)$ during the freezing interval, and is taken to be constant since freezing occurs over a very narrow S_i range [*Kärcher and Lohmann*, 2002b] and N_c is usually much less than N_o [i.e., *Lin, et al.*, 2002]. Since in a monotonically increasing S_i field $P_f(S_o^{'})$ decreases with increasing D_c (as explained below), a negative sign is introduced in equation (13).

Calculation of $S_o^{'}$ is key for solving equation (13); this is done by combining equations (1) and (2),

$$\frac{dS_i}{dt} = \alpha V S_i - \beta \frac{dw_i}{dt} \tag{14}$$

where $\alpha = \frac{g\Delta H_s M_w}{c_p R T^2} - \frac{g M_a}{RT}$, $\beta = \frac{M_a p}{M_w p_i^o} >> \frac{\Delta H_s^2 M_w}{c_p R T^2}$. Before the nucleated ice crystals substantially impact saturation ("free growth", Figure 3), $\frac{dw_i}{dt} \approx 0$, and the integration of (14) from $S_o^{'}$ to $S_{i,max}$ gives

$$t - t_o \approx \frac{1}{\alpha V}\left(1 - \frac{S_o^{'}}{S_{i,\max}}\right) \tag{15}$$

where the approximation $\ln(x) \approx x - 1$ has been used. Equation (15) is similar to the "upper bound" expression derived by *Twomey* [1959] for liquid water clouds. Numerical simulations (section 4) support that "free growth" holds up to S_i values very close $S_{i,\max}$; for $S_i \rightarrow S_{i,max}$ however, equation (15) may underestimate t-t_o and its effect is discussed in section 4.

By definition, t-t_o should equal the time for growth of the ice particles from D_o to D_c (Figure 3), which is found by integration of (5),

$$t - t_o = \frac{1}{(S_i - 1)}\left[\frac{\Gamma_1}{2}(D_c^2 - D_o^2) + \Gamma_2 (D_c - D_o)\right] \tag{16}$$

where S_i has been assumed as constant as nucleation occurs in a very narrow S_i range (i.e., Figure 5). The calculation of $P_f(S_o^{'})$ using equation (9) requires the knowledge of J as an explicit function of S_i; this can be further simplified given that nucleation occurs on

a very narrow interval of saturation so that $J(S_i)$ can be approximated related to $J(S_{i,max})$ [i.e., *Seinfeld and Pandis*, 1998; *Khvorostyanov and Curry*, 2005] as

$$\ln\frac{J(S_i)}{J(S_{i,\max})} \approx k(T)\left(S_i - S_{i,\max}\right) \tag{17}$$

$k(T)$ is obtained by fitting the *Koop et al.* [2000] data for J between 10^8 and 10^{22} $m^{-3}s^{-1}$,

$$k(T) = 0.01046T^2 - 3.489T + 405.6 \tag{18}$$

with T in K. Using (14) and (17), (9) is solved under the assumption of free growth to give

$$P_f(D_o, S_o^{'}) \approx \frac{1}{\alpha V S_{i,\max}} \int_{S_o}^{S_o^{'}} v_o J(S) dS = \frac{J(S_{i,\max}) v_o}{\alpha V\, k(T) S_{i,\max}} \exp\left[-k(T)(S_{i,\max} - S_o^{'})\right] \tag{19}$$

where $v_o = \frac{\pi D_o^3}{6}$, and the approximation $1 - \exp\left(-\int_0^t v_o J(t)dt\right) \approx \int_0^t v_o J(t)dt$ has been used.

The lower integration limit, S_o, in (19) represents the beginning of the freezing pulse, assumed to be where $P_f(D_o, S_o) < 10^{-6} P_f(D_o, S_{i,\max})$, i.e., $\exp\left[-k(T)(S_{i,\max} - S_o^{'})\right] >> \exp\left[-k(T)(S_{i,\max} - S_o)\right]$. The integration is not very sensitive to the latter assumption, as most of the ice crystals form for S_i close to $S_{i,max}$ [i.e., *Kärcher and Lohmann*, 2002a]. Combining (15) and (16) to find $S_{i,\max} - S_o^{'}$, and replacing into (19) gives

$$P_f(D_o, D_c) = \frac{J(S_{i,\max}) v_o}{\alpha V\, k(T)\, S_{i,\max}} \exp\left[-\mu \Gamma(D_c, D_o)\right] \tag{20}$$

where $\mu = \frac{\alpha V\, k(T)\, S_{i.\max}}{(S_{i.\max} - 1)}$, and $\Gamma(D_c, D_o) = \frac{\Gamma_1}{2}(D_c^2 - D_o^2) + \Gamma_2(D_c - D_o)$. The ice number distribution function at $S_{i,max}$ is obtained after computing $\frac{\partial P_f(D_o, D_c)}{\partial D_c}$ from (20) and substituting into (13)

$$n_c(D_c, D_o)\big|_{S_{i,\max}} = \overline{n}_o(D_o)\frac{J(S_{i,\max})v_o}{(S_{i,\max} - 1)}\left(\Gamma_1 D_c + \Gamma_2\right)\exp\left[-\mu\Gamma(D_c, D_o)\right] \qquad (21)$$

Since ice particles attain large sizes after freezing, the spectrum of D_c values spans over several orders of magnitude [i.e., *DeMott, et al.*, 1994; *Monier, et al.*, 2006]. Typically variation in D_o is much smaller; furthermore, P_f reaches significant values only in a fraction of the liquid droplets (generally those with larger sizes and low solute concentrations [*Pruppacher and Klett*, 1997]). With this, the value of $\exp\left[-\mu\Gamma(D_c, D_o)\right]$ will be dominated by variation in D_c, and the approximation $\exp\left[-\mu\Gamma(D_c, D_o)\right] \approx \exp\left[-\mu\Gamma(D_c, \overline{D}_o)\right]$ can be used. Obtaining the crystal size distribution then is done by integration of (21) over the contribution from each droplet size class,

$$n_c(D_c)\big|_{S_{i,\max}} = \frac{J(S_{i,\max})}{(S_{i,\max} - 1)}\left(\Gamma_1 D_c + \Gamma_2\right)\exp\left[-\mu\Gamma(D_c, \overline{D}_o)\right]\int \overline{n}_o(D_o)v_o dD_o \qquad (22)$$

which for a lognormal distribution of $\overline{n}_o(D_o)$ gives

$$n_c(D_c)\big|_{S_{i,\max}} = \frac{N_o \overline{v}_o e^{9/2\ln^2\sigma_g} J(S_{i,\max})}{(S_{i,\max} - 1)}\left(\Gamma_1 D_c + \Gamma_2\right)\exp\left[-\mu\Gamma(D_c, \overline{D}_o)\right] \qquad (23a)$$

or

$$n_c(\ln D_c)\big|_{S_{i,\max}} = \left.\frac{dN_c}{d\ln D_c}\right|_{S_{i,\max}} = \frac{N_o \bar{v}_o e^{9/2\ln^2\sigma_g} D_c J(S_{i,\max})}{(S_{i,\max}-1)}\left(\Gamma_1 D_c + \Gamma_2\right)\exp\left[-\mu\Gamma(D_c, \overline{D}_o)\right] \quad (23b)$$

where $\bar{v}_o = \frac{\pi}{6}\overline{D}_o^3$ and σ_g is the geometric dispersion of the droplet size distribution. Equation (23) is the final expression used for the size distribution of the ice crystals at $S_{i,max}$. Equations (21-23) demonstrate the probabilistic character of ice nucleation: at any time particles of all sizes have finite freezing probabilities; i.e., the population of ice crystals of a given size D_c results from the freezing of droplets with different sizes. From this, the freezing of a monodisperse aerosol size population produces a polydisperse ice crystal population. Since for values below $S_{i,max}$, S_i increases monotonically with time, the number of crystals generally increases as D_c decreases. For a given droplet size, $P_f(D_o, S_i)$ will increase with time so that the number of newly formed crystals will increase. These crystals in turn will have less time to grow before S_i reaches $S_{i,max}$; that is, the most recently formed crystals will have the largest probability of freezing, i.e., $P_f(D_c = \overline{D}_o, S_{i,\max})$. The maximum in the distribution may be shifted to $D_c > \overline{D}_o$ if the time scale for the growth of the newly formed particles is larger than the timescale of change of probability (see section 4).

3.2 Calculation of N_c at $S_{i,max}$

The deposition rate of water vapor upon ice crystals can be approximated by substituting equation (23) into (4),

401 $$\frac{dw_i}{dt} = \frac{\rho_i}{\rho_a}\frac{\pi}{2} N_o \bar{v}_o e^{9/2\ln^2\sigma_g} J(S_{i,\max}) \int_{D_o}^{Dc,s_{\max}} D_c^2 \exp\left[-\frac{\mu}{2\overline{\Gamma}}(D_c^2 - \overline{D}_o^2)\right] dD_c \qquad (24)$$

402 where $D_{c,s_{\max}}$ is the equivalent diameter of the largest ice crystal at $S_{i,\max}$ (calculated in

403 section 3.3) and $\overline{\Gamma}$ is given by [i.e., *Fountoukis and Nenes*, 2005]

404 $$\overline{\Gamma} = \frac{\int_{\overline{D}_o}^{Dc,s_{\max}} \frac{D_c}{\Gamma_1 D_c + \Gamma_2} dD_c}{D_{c,s_{\max}} - \overline{D}_o} = \frac{1}{\Gamma_1}\left[1 + \frac{\Gamma_2}{\Gamma_1}\frac{\ln\left(\frac{\Gamma_2 + \Gamma_1 D_{c,s_{\max}}}{\Gamma_2 + \Gamma_1 \overline{D}_o}\right)}{D_{c,s_{\max}} - \overline{D}_o}\right] \qquad (25)$$

405 Integration of (24) gives

406 $$\frac{dw_i}{dt} = \frac{\rho_i}{\rho_a}\frac{\pi}{2} N_o \bar{v}_o e^{9/2\ln^2\sigma_g} J(S_{i,\max}) \frac{e^{\frac{\mu}{2\overline{\Gamma}}\overline{D}_o^2}}{4\left(\frac{\mu}{2\overline{\Gamma}}\right)^{3/2}} \left[\sqrt{\pi}\, erf\left(\sqrt{\frac{\mu}{2\overline{\Gamma}}} D_c\right) - 2\sqrt{\frac{\mu}{2\overline{\Gamma}}}\, D_c e^{-\frac{\mu}{2\overline{\Gamma}}D_c^2}\right]_{\overline{D}_o}^{D_{c,s_{\max}}}$$

407 (26a)

408 An order of magnitude estimation of parameters based on parcel simulations (not shown)

409 suggest that $\overline{D}_o \sim 10^{-7}$ m, $D_{c,s_{\max}} \sim 10^{-5}$ m and $\frac{\mu}{2\overline{\Gamma}} \sim 10^{10}$ m^{-2}. Therefore, the term in

410 brackets in (26a) tends to approach $\sqrt{\pi}$ in most conditions, i.e.,

411 $$\frac{dw_i}{dt} = \frac{\rho_i}{\rho_a} N_o \bar{v}_o e^{9/2\ln^2\sigma_g} J(S_{i,\max}) \frac{e^{\frac{\mu}{2\overline{\Gamma}}\overline{D}_o^2}}{\left(\frac{2\mu}{\pi\overline{\Gamma}}\right)^{3/2}} \qquad (26b)$$

412 after substitution of (26b) into (14), at $\frac{dS_i}{dt} = 0$,

413 $$\alpha V S_{i,\max} = \beta \frac{\rho_i}{\rho_a} N_o \bar{v}_o e^{9/2\ln^2\sigma_g} J(S_{i,\max}) \frac{e^{\frac{\mu}{2\overline{\Gamma}}\overline{D}_o^2}}{\left(\frac{2\mu}{\pi\overline{\Gamma}}\right)^{3/2}} \qquad (27)$$

414 the fraction of frozen particles, f_c, at $S_{i,\,max}$ is found at the maximum P_f, given by (20)

415 $$f_c = \frac{1}{N_o}\int \overline{n}_o(D_o)P_f(D_c = \overline{D}_o, \overline{D}_o)dD_o = \frac{\overline{v}_o e^{9/2\ln^2\sigma_g} J(S_{i,\max})}{\alpha V S_{i,\max}} \quad (28)$$

416 combining (27) and (28) we arrive at,

417 $$f_c = \frac{\rho_a}{\rho_i}\frac{[k(T)]^{1/2}}{\beta N_o}\left[\frac{2\alpha V S_{i,\max}}{\pi\overline{\Gamma}(S_{i,\max}-1)}\right]^{3/2}\exp\left[-\frac{\alpha V k(T) S_{i,\max}}{2\overline{\Gamma}(S_{i,\max}-1)}\overline{D}_o^2\right] \quad (29)$$

418

419 The exponential term in (29) approaches unity, which is a result of the assumption made
420 in (13) that freezing depletes a negligible amount of aerosol (i.e., $\overline{n}_o(D_o)$ is constant
421 during the nucleation process). Since the term $J(S_{i,max})$ has been eliminated from (29), f_c is
422 not strongly influenced by small variations in $S_{i,max}$. Thus, $S_{i,max}$ can be taken as the
423 saturation freezing threshold obtained solving the *Koop et. al.* [2000] parameterization
424 for $J(S_{i,\max}) = 10^{16}$ s^{-1} m^{-3}, which is close to the nucleation rate of pure water at -38 °C
425 [*Pruppacher and Klett*, 1997; *Sassen and Benson*, 2000], and represents an average of
426 $J(S_{i,\max})$ over a wide set of simulations (section 4). The total number of crystals would be
427 given by, $N_c = N_o f_c$, however such result will not be constrained by N_o as upper limit.
428 Instead, purposely contradicting the assumption made in (19), f_c can be associated with
429 the solution of the integral in (9), i.e., $f_c \approx \int_0^t v_o J(t)dt$ and then write

430 $$N_c = N_o e^{-f_c}(1 - e^{-f_c}) \quad (30)$$

431 where $N_o e^{-f_c}$ represents the number of remaining unfrozen droplets.

432

433

3.3 Calculation of $D_{c,s_{\max}}$

$D_{c,s_{\max}}$ is required for calculating the ice growth rate (equation (26b)); Two methods are developed to calculate it. The first one is based on theoretical arguments, and assumes $D_{c,s_{\max}}$ as the diameter of the ice crystal at which $\frac{P_f(D_c = D_o, D_o)}{P_f(D_c, D_o)} = 10^{-6}$ (i.e., the size above which the number of crystals is below $10^{-6}N_c$). With this, equation (20) can be solved for $D_{c,s_{\max}}$,

$$D_{c,s_{\max}}^2 + \frac{2\Gamma_2}{\Gamma_1} D_{c,s_{\max}} - \frac{2\ln(10^{-6})(S_{i,\max} - 1)}{\alpha V k(T) S_{i,\max} \Gamma_1} = 0 \qquad (31)$$

where we have assumed $D_{c,s_{\max}} >> D_o$ (supported by numerical simulations). Since $\Gamma_2 \propto \frac{1}{\alpha_d}$ (Equation (6)), the value of $D_{c,s_{\max}}$ would increase as α_d decreases. For low values of α_d ice crystals grow slowly, and non-continuum effects limit the condensation rate; when ice become large enough, gas-to-particle mass transfer is in the continuum regime and the crystals grow quickly [*Pruppacher and Klett*, 1997]. When growth of the newly frozen ice crystals is delayed, water vapor water tends to condensate preferentially to preexisting ice crystals. Slow uptake effects became important for α_d lower than 0.1, i.e, when Γ_1 becomes comparable to Γ_2 [*Lin, et al.*, 2002; *Gierens, et al.*, 2003]. Alternatively, $D_{c,s_{\max}}$ can be computed using an empirical fit to numerical simulations obtained with the parcel model,

$$D_{c,s_{\max}} = \min\left\{(1.6397\times10^{-14}T - 3.1769\times10^{-12})V^{-0.05}(N_o D_{g,dry}^3)^{-0.373};\ 10^{-4}\right\} \qquad (32)$$

where V is in m s^{-1}, T is in K, N_o in cm^{-3} and $D_{g,\,dry}$ in m. Equation (30) was generated over a broad set of T, p, V, N_o, $D_{g,\,dry}$, and α_d (Table 1, section 4). The T and V

454 dependencies in (32) are introduced to adjust the effective growth of the particles
455 correcting for the "free growth" assumption (section 3.1). Additional variability not taken
456 into account in the formulation of (30) is caused by the effect of variation in the aerosol
457 properties. Since $n_o(D_o)$ is in equilibrium with the dry aerosol size distribution, an
458 increase $D_{g,\,dry}$ will increase the total volume of the liquid aerosol particles therefore
459 increasing P_f. This would produce a longer freezing pulse and increase N_c. The same
460 effect can be achieved by reducing the effective growth of the particles, which explains
461 the approximated dependency of $D_{c,Smax}$ on the average volume of the dry aerosol
462 population, i.e., $\sim \left(N_o D_{g,dry}^3\right)^{1/3}$ (equation (32)).
463
464 **3.4 Implementation of the Parameterization**
465 The application of the parameterization is presented in Figure 4. As input, one requires
466 the conditions of cloud formation T, P, V, and α_d and the aerosol characteristics (i.e., N_o
467 and $D_{g,dry}$); the outputs are N_c and size distribution information. To apply the
468 parameterization, first $\overline{\Gamma}$ is calculated (Equation (25)) using $D_{c,s_{\max}}$ estimated using either
469 Equation (31) or (32), the latter being preferred. $S_{i,max}$ is obtained by solving
470 $J(S_{i,\max}) = 10^{16}$ s^{-1} m^{-3} [*Koop, et al.*, 2000], for which reported fits, relating $S_{\mathrm{i,max}}$ at
471 $J(S_{i,\max}) = 10^{16}$ s^{-1} m^{-3} to T, can be employed [i.e., *Ren and Mackenzie*, 2005]. N_c is
472 calculated from (30) using f_c calculated from (29). After f_c is calculated, $J(S_{i,\max})$ can be
473 corrected using $J(S_{i,\max}) = \dfrac{f_c \alpha V S_{i,\max}}{\bar{v}_o e^{9/2\ln^2\sigma_g}}$ (equation (27)) from where $n_c(D_c, D_o)$ is obtained
474 (equations (21-23)). There is still uncertainty regarding the values of α_d and the aerosol

475 characteristics [*Lin, et al.*, 2002]; the sensitivity of the parameterization results to these
476 parameters is discussed in the next section.
477

478 4 Evaluation of the Parameterization

479 The parameterization was evaluated against the detailed numerical solution of the parcel
480 model over a wide range of T, V, $D_{g,\,dry}$, N_o, and α_d (Table 1), in a total of 1200 runs,
481 covering the expected variation in cirrus cloud formation conditions in a GCM
482 simulation. The parcel model was run using initial $S_i = 1.0$; initial p was estimated as in
483 hydrostatic equilibrium at T using a dry adiabatic lapse rate. The dry aerosol population
484 was assumed to be pure H_2SO_4, lognormally distributed. To test aged, unperturbed, and
485 perturbed aerosol runs the geometric dispersion of the dry aerosol distribution, $\sigma_{g,\,dry}$ was
486 selected to be 1.7, 2.3 and 2.9 respectively [*Seinfeld and Pandis*, 1998]. The liquid
487 aerosol was assumed to be in equilibrium with S_i in all simulations. Calculated N_c ranged
488 from 0.001 to 100 cm^{-3} and $S_{i,\max}$ varied between 1.4 and 1.6 which agrees the range on
489 reported values for cirrus formation by homogeneous freezing [i.e., *Heymsfield and*
490 *Sabin*, 1989; *Lin, et al.*, 2002].
491

492 Two main assumptions were introduced in the development of the parameterization, i.e.,
493 the calculation of N_c at $S_{i,max}$ rather than at the end of the freezing pulse, i.e.,
494 $N_c \approx N_c\big|_{S_{\max}}$; and the assumption of negligible impact of the newly formed crystals on S_i
495 before $S_{i,max}$ is reached ("free growth"). Figure 5 shows how these assumptions may
496 impact the results of the parameterization for high and low V and T (1-0.04 m s^{-1}, 233-
497 203 K). By using free growth regime to estimate the evolution of S_i (dotted black line),

498 $S_{i,max}$ is overestimated by about 0.5 % at low V (bottom left) to about 2% at high V (top
499 right). At high T (right panels) such overestimation is not expected to exert a large
500 influence in the performance of the parameterization as low values of $S_{i,max}$ are reached.
501 Therefore the small overestimation in $S_{i,max}$ will not significantly influence $J(S_{i,max})$
502 (which is a very nonlinear function $S_{i,max}$). However, as T decreases and V increases, $S_{i,max}$
503 reaches higher values during the parcel ascent and small changes in $S_{i,max}$ significantly
504 impact J (hence P_f), for which an overestimation in N_c may be expected. Conversely,
505 Figure 5 shows that at low V (bottom panels), $N_c\big|_{S_{\max}}$ underestimates the actual N_c by
506 nearly a factor of 2; since few ice crystals (low $S_{i,max}$) are formed, it takes a longer time to
507 deplete the available water vapor resulting in longer freezing pulses. At high V (top
508 panels) $N_c\big|_{S_{\max}}$ is close to N_c, since $S_{i,max}$ is reached rapidly and a larger number of crystals
509 is formed; this effect will be more important at low T as higher $S_{i,max}$ values are reached .
510
511 **4.1 Calculation of $n_c(D_c)$**
512 The parameterized $n_c(D_c)$, equation (23b), is presented for two representative cases in
513 Figure 6, along with $n_c(D_c)\big|_{S_{i\max}}$ obtained from parcel model simulations. Although the
514 effect of the droplet size distribution parameters is explicitly considered in (23) it cancels
515 out with its effect on f_c (which is a result of the assumption constant $\overline{n}_o(D_o)$), and a
516 single crystal size distribution is obtained for the three values of $\sigma_{g,\,dry}$ tested (although
517 small variations in $n_c(D_c)\big|_{S_{i\max}}$ may occur due to differences in T at $S_{\mathrm{i,max}}$), this is not
518 critical as N_c variations with respect to $\sigma_{g,\,dry}$ are generally small (i.e., Figure 6). $\overline{D}_o$ was

assumed as the equilibrium size of $D_{g,\ dry}$ at $S_{i,\ max}$. $n_c(D_c)$ was calculated using the procedure outlined in section 3.4 (Figure 4) in which $J(S_{\mathrm{i,max}})$ is corrected using equations (30) and (32) (therefore enforcing $N_c \approx \int_{D_c=\overline{D}_o}^{D_{c,\max}} n_c(D_c)\,dD_c$). Generally, the parameterized $n_c(D_c)$ reproduces well the numerical results at $S_{i,max}$, however, it predicts a continuous size distribution down to $\overline{D}_o$, which differs from the numerical results. This can be explained due to the discrete nature of the size distribution (and of the numerical method). After freezing, the newly formed ice crystals "jump" to larger sizes leaving gaps in the distribution, and eliminating part of the left-tail of the size distribution. Due to the continuous nature of the parameterized $n_c(D_c)$, it would tend to overpredict $N_c\big|_{S_{\max}}$. The adjusted $J(S_{\mathrm{i,max}})$ will then be slightly below the obtained in numerical simulations to satisfy $N_c = N_c\big|_{S_{\max}}$. This works well in the cold case (T=213, V=1 m s^{-1}, Figure 6, left) as more crystals are to be produced after $S_{i,\ max}$ is reached. However in the warm case (T=233, V=0.2 m s^{-1}, Figure 6, right), the freezing pulse is shorter and the correction in $J(S_{\mathrm{i,max}})$ produces a reduction in the peak of the distribution. The influence of these factors on the resulting effective radius of the cirrus cloud, and its radiative properties, will require the time integration of $n_c(D_c)$, and the comparison with numerical simulations at different stages after cloud formation. Although such a task may be readily achieved, it is out of the focus of this manuscript and will be undertaken in future works.

4.2 Calculation of N_c

Figure 7 shows the comparison of N_c predicted by the parcel model and the parameterization, equation (30), using the theoretical calculation of $D_{c,s_{\max}}$ (right, equation (31)) and using the empirical correlation for $D_{c,s_{\max}}$ (left, equation (32)). The effects of the assumption of "free growth" and the approximation of N_c as $N_c\big|_{S_{\max}}$ are expected to cancel out at moderate T and V. However at low V and high T (hence low N_c), the parameterization tends to underestimate N_c with respect to the parcel model results; the opposite tendency occurs at very high V (>2 m s^{-1}) and low T (hence, high N_c). This latter is not significant as such conditions are not typical of cirrus formation [i.e., *Heymsfield and Sabin*, 1989; *Gayet, et al.*, 2004]. In summary, using the theoretically calculated $D_{c,s_{\max}}$ gives a parameterized N_c always within a factor of 2 of the N_c predicted by the parcel model with a mean relative error about -15% (for all runs in Table 1). When using the empirically calculated $D_{c,s_{\max}}$ (equation (32)) is used, the parameterized N_c is much closer to the numerical parcel model (average relative error 1% ± 28%), as equation (32) allows more flexibility in reproducing the parcel model results, and accounts for the additional variability due to effect of aerosol size and number.

4.3 Comparison Against Other Parameterizations

The parameterization results were compared to those of several reported works for different combinations of V, N_o, $D_{g,\,dry}$, T, and α_d. The parameterizations used in this section are those of *Liu and Penner* [2005 , hereafter LP2005], *Sassen and Benson* [2000, hereafter SB2000], and *Kärcher and Lohmann*, [2002a, hereafter, KL2002; *Fountoukis*

562 *and Nenes*, 2005]. SB2000 is based on an empirical fit to numerical simulations relating
563 N_c to T and V. A similar approach is used in LP2005 where an additional dependency on
564 N_o is included. In both cases, J is calculated through classical nucleation theory (the latter
565 using the effective temperature method [i.e., *DeMott, et al.*, 1994]). KL2002 is physically
566 based and employs the freezing timescale and the threshold supersaturation as input
567 parameters. It resolves explicitly the dependency of N_c on T, V, α_d, and D_o, and uses N_o as
568 upper limit for N_c. Although the freezing of polydisperse aerosol is discussed in KL2002
569 not explicit solution is presented, therefore their monodisperse solution is used for
570 comparison. The freezing timescale and supersaturation threshold are calculated using the
571 analytical fits to *Koop et al.* [2000] data provided by *Ren and Mackenzie* [2005]. $\overline{D}_o$ in
572 this case was taken as in equilibrium with the volume-weighted geometric mean diameter
573 of the dry size distribution. By using this definition of $\overline{D}_o$, the best agreement between
574 the parcel model simulations and the results of the KL2002 parameterization was
575 obtained. The three parameterizations were compared to the solution of equation (30)
576 using theoretically calculated $D_{c,max}$, equation (31) (termed "theoretical", still $k(T)$,
577 equation (18), has been derived from an empirical fit to J), and using the empirically
578 adjusted $D_{c,max}$ equation (32), (termed "adjusted"). $\overline{D}_o$ was calculated as the equilibrium
579 size of $D_{g,\,dry}$ at $S_{i,\,max}$. All parameterizations are evaluated using T obtained at $S_{i,max}$ from
580 the parcel model simulations. α_d was set to 0.1 and 1.0 to test both diffusionally and non-
581 difussionally limited cases (see section 3.3).
582
583
584

585 *Dependency on V*

586 Figure 8 presents the comparison of the different parameterizations at T_o= 213 (left panel,
587 T between 208.6 and 209.4 K) and 233 K (right panel, T between 228.8 and 229.2 K),
588 and α_d = 0.1 (black) and 1.0 (blue). At T_o=233 K, all parameterizations agree fairly well
589 when α_d = 0.1 and V < 1 m s^{-1}. At higher V, KL2002 and LP2005 predict a larger N_c,
590 whereas SB2000 predicts a lower N_c, with respect to the parcel model results, although
591 the difference becomes significant only for V > 3 m s^{-1}. At these conditions the adjusted
592 parameterization follows well the parcel model results whereas the theoretical
593 parameterization slightly underpredicts N_c at low V. Runs made using α_d =1 (blue)
594 showed a good agreement between KL2002, the adjusted and theoretical
595 parameterizations, and the numerical results. This is expected as equation (28) bears the
596 same dependency on V and p_i^o, reported by KL2002 in their "fast growth" solution (i.e.,
597 $N_c \propto V^{3/2}$) and emphasized by more recent works [*Gierens*, 2003; *Ren and Mackenzie*,
598 2005]. At high f_c (i.e., low T, low α_d, and high V) the exponential term in (30) dampens
599 the effect of V (also due to the dependency of $D_{c,s_{\max}}$ on V) and N_c becomes almost linear
600 on V. Results at α_d = 1 lie below those of LP2005 and SB2000, who used lower α_d values
601 for their numerical simulations (LP2005 used α_d = 0.1 and SB2000 used α_d = 0.36 [*Lin, et*
602 *al.*, 2002]). At T_o=213 K, and α_d = 0.1 (left, black), the parameterizations agree only for V
603 below 0.3 m s^{1} whereas for large V they diverge, being N_c calculated using KL2002, the
604 largest over the whole V interval. At very high V (>3 m s^{-1}) the adjusted parameterization
605 underpredicts N_c with respect to the parcel model results which is a result of the
606 exponential term introduced in (30). As with T_o = 233 K, KL2002, and the adjusted and

607 theoretical parameterizations agree well with the numerical results when α_d = 1, and
608 T_o=213 K (left, blue).
609
610 *Dependency on N_o*
611 Figure 9 presents N_c as a function of N_o for V=0.2 m s^{-1} (left) and V=1.0 m s^{-1} (right) and
612 T_o=213 (black) and 233 K (blue); for these simulations $D_{g,dry}$ was set to 40 nm and α_d to
613 0.1. In all cases of Figure 9, LP2005 and the adjusted parameterization show the best
614 agreement with the parcel model results. Still, at T_o=213 K, V= 1.0 m s^{-1}, the adjusted
615 parameterization underpredicts with respect to the numerical results, for N_o below 20 cm^{-}
616 ^{3} whereas LP2005 overpredicts; in both cases the difference with the parcel model results
617 is about ± 50 %, which is not critical as these very low N_o are atypical of cirrus forming
618 conditions [i.e., *Pruppacher and Klett*, 1997]. In all cases of figure 9 KL2002 predicts a
619 larger N_c than the parcel model, however the difference becomes much smaller at large
620 N_o. In the same interval of N_o, SB2000 predicts N_c close to the average of the parcel
621 model results at T_o=213 K; when T_o=233 K, SB2000 predicts N_c close to the parcel model
622 results at large N_o. The theoretical parameterization shows the opposite tendency and
623 tends to agree better with the parcel model results at low N_o. In most of the cases the
624 parcel model results can be reasonable well fitted in the form $N_c = aN_o^b$ where a and b
625 are functions of T, V, $D_{g,\,dry}$ and α_d (also proposed in LP2005). The dependency of N_c on
626 N_o generally increases when T and α_d decrease, and V increases. For the cases of Figure 9,
627 b lies between 0.19 (T_o=233 K , V= 0.2 m s^{-1}) and 0.61 (T_o=213 K , V= 1 m s^{-1}). This is
628 in good agreement with experimental and numerical studies that usually report an

629 increase in N_c by a factor between 2 and 4 for a 10-fold increase in N_o [i.e., *Heymsfield*
630 *and Sabin*, 1989; *Jensen and Toon*, 1994; *Seifert, et al.*, 2004].
631
632 *Dependency on* $D_{g,\,dry}$
633 Figure 10 presents N_c as a function of $D_{g,\,dry}$ for T_o=213 (left) and T_o=233 (right), and α_d
634 = 0.1 (black) and α_d = 1 (blue); for these simulations V=1.0 m s^{-1} and N_o = 200 cm^{-3}. To
635 apply KL2002, $D_{g,\,dry}$ was converted into the volume-weighted mean diameter in
636 equilibrium with $S_{i,max}$; however N_c results in Figure 10 are plotted using the original $D_{g,}$
637 $_{dry}$. In all conditions of Figure 10 parcel model results suggest an approximated linear
638 dependency of N_c with $D_{g,\,dry}$, which is also found by the combination of equations (29)
639 and (32). This is a result of the increased P_f due to the larger volume of the liquid aerosol
640 particles in equilibrium with the aerosol dry distribution (see section 3.3 and equation
641 (9)), which was also observed in LP2005. This result is opposite to the tendency
642 predicted by KL2002 ($N_c \propto \overline{D}_o^{-1}$), and also (although much more slightly) by the
643 theoretical parameterization. In the latter, the effect of increased P_f is not accounted for
644 due to the assumption of an infinite aerosol source (section 3.1, equation (13)). Although
645 LP2005 does not take into account this dependency it predicts N_c in agreement with
646 parcel model results at $D_{g,\,dry}$ = 80 nm, and α_d = 0.1. SB2000 predicted N_c agrees with the
647 parcel model results at $D_{g,\,dry}$ = 40 nm and T_o=213, and at $D_{g,\,dry}$ = 120 nm and T_o=233,
648 when α_d = 0.1. If a linear fit is adjusted to the cases shown in Figure 10 then its slope will
649 decrease from 0.32 at T_o=213 and α_d = 0.1 to 0.015 at T_o=233 and α_d = 1, which indicates
650 again that these effects would be more important at low T and high V. In all cases of
651 Figure 10 the adjusted parameterization reproduces closely the parcel model results.

While the comparison of the different parameterizations was carried out over a comprehensive set of conditions, common values of $D_{g,\,dry}$ often vary between 40-100 nm (and between 100-500 cm^{-3} for N_o) [e.g., *Heymsfield and Miloshevich*, 1995; *Gayet, et al.*, 2004]. Figures 8-10 show that the effect of T and V variations on N_c is much stronger than that of $D_{g,\,dry}$ and N_o. The relative importance of each parameter remains to be assessed in global model studies.

5 Summary and Conclusions

To address the need for improved physics of ice cloud formation in large scale models, we have developed a parameterization for cirrus clouds formation, which is robust, computationally efficient, and links chemical effects (e.g., water activity and uptake effects) with ice formation via homogenous freezing. This was accomplished by tracing back the growth of ice crystals to their point of freezing, in a given ice saturation profile, connecting their size to their freezing probability. Using this approach, an expression for the crystal size distribution is derived, the integration of which yields the number concentration of crystals, and compared against the solution of a detailed parcel model. The numerical solution of the parcel model was accomplished by using a Lagrangian particle tracking scheme. In this method the evolution of the ice crystal size distribution is described by the superposition and growth of monodisperse crystal populations generated by the freezing of single classes (of same size and composition) of supercooled droplets.

674 The parameterized ice crystal size distribution captured well the characteristics of the ice
675 crystal population and represents a robust approximation to calculate N_c. Its integration to
676 find N_c was carried out either using complete theoretical arguments or their combination
677 with parcel model results. When compared against the predictions of the numerical parcel
678 model over a broad set of conditions, the theoretically based parameterization for N_c
679 reproduced the results of the parcel model within a factor of two and with an average
680 relative error of about -15%. Adjustments in the ice crystal growth rate (using numerical
681 simulations) further reduced the relative error to 1 ± 28%, which is remarkable given the
682 simplicity of the final expression obtained for N_c, the broad set of conditions tested, and
683 the complexity of the parcel model equations.
684
685 Due to its analytical nature the proposed parameterization presented in this work offers
686 explicitly relation between variables, that as analyzed in the last section goes beyond
687 scaling factors, and it is not constrained to a single set of parameters (i.e., α_d, aerosol
688 characteristics) which is desirable due to the large uncertainty associated with them. As
689 shown in Figure 7 the accuracy with which the parameterization reproduces the parcel
690 model results, is independent of these parameters. In this regards, only the KL2002
691 parameterization shares this advantages, however the presented parameterization offers
692 explicitly the relation between the different variables that determine the freezing time
693 scale of the particles, and explicitly considers the effect of the aerosol number on N_c.
694
695 This work offers a new, alternative approach to the description of cirrus formation and its
696 representation in large scale models. The results given are applicable for cirrus formation

on predominantly homogenous freezing conditions. Still, in a number of cases heterogeneous freezing and competition between multiple particle types significantly affect the cloud formation process. Both the numerical model and the parameterization can be readily extended to include these effects, which will be the focus of future work.

6 Acknowledgments

This study was supported by NASA MAP, NASA EOS-IDS-CACTUS, and a NASA New Investigator Award. We would also like to thank Dr. B.Kahn for his comments on the manuscript.

APPENDIX

List of Symbols

α, β	Parameters defined in equation (14)
α_d	Water vapor to ice deposition coefficient
c_p	Heat capacity of air
ΔH_s	Heat of sublimation of water
$D_{c,s_{\max}}$	Diameter of the largest ice particle at $S_{i,max}$
D_c	Volume sphere-equivalent diameter of an ice particle
$D_{g,\,dry}$	Geometric mean diameter of the dry aerosol size distribution
D_o	Diameter of a liquid aerosol particle
D_v	Bulk water vapor diffusion coefficient

f_c	Fraction of frozen particles at $S_{i,max}$
g	Acceleration of gravity
$\Gamma(D_c, D_o)$	Growth function defined in equation (20)
$\overline{\Gamma}$	Effective growth parameter defined in equation (25)
$\Gamma_1,\ \Gamma_2$	Parameters defined in equation (6).
J	Nucleation rate coefficient
$k(T)$	Constant defined in equation (18)
k_a	Thermal conductivity of air
μ	Parameter defined in equation (20)
$M_w,\ M_a$	Molar masses of water and air, respectively
$n_c(D_c, D_o)$	Ice crystal number distribution function originated at D_o
$n_c(D_c)$	Ice crystal number distribution function
$n_o(D_o)$	Liquid aerosol size distribution function
$\overline{n}_o(D_o)$	Average liquid aerosol size distribution function during freezing
$N_c\big\vert_{S_{\max}}$	Ice crystal number concentration at $S_{i,max}$
N_c	Ice crystal number concentration
N_o	Aerosol number concentration
p	Ambient pressure
p_i^o	Ice saturation vapor pressure
$P_f,\ P_f(D_o, t)$	Cumulative probability of freezing
ρ_i, ρ_a	Ice and air densities, respectively

R	Universal gas constant
σ_g	Geometric dispersion of the liquid aerosol size distribution
$\sigma_{g,\ dry}$	Geometric dispersion of the dry aerosol size distribution
S_i	Water vapor saturation ratio with respect to ice
$S_{i,eq}$	Equilibrium ice saturation ratio
$S_{i,max}$	Maximum ice saturation ratio
S_o	Ice saturation ratio at the beginning of freezing
S_o'	Ice saturation ratio at which an ice crystal was formed
T	Temperature
t	Time
t_o	Time of freezing
V	Updraft velocity
v_o	Volume of a liquid droplet of size D_o
w_i	Ice mass mixing ratio
$\psi(D_o,t)$	Ice nucleation function

7 References

Abbatt, J. P. D., S. Benz, D. J. Cziczo, Z. Kanji, and O. Möhler (2006), Solid ammonium sulfate as ice nuclei: a pathway for cirrus cloud formation, *Science*, *313*, 1770-1773.

Archuleta, C. M., P. J. DeMott, and S. M. Kreidenweis (2005), Ice nucleation by surrogates for atmospheric mineral dust and mineral dust/sulfate particles at cirrus temperatures, *Atmos. Chem. Phys.*, *5*, 2617-2634.

Cantrell, W., and A. J. Heymsfield (2005), Production of ice in tropospheric clouds, *Bull. Am. Meteorol. Soc.*, *86*, 795-807.

Chen, Y., P. J. DeMott, S. M. Kreidenweis, D. C. Rogers, and D. E. Sherman (2000), Ice formation by sulfate and sulfuric acid aerosol particles under upper-tropospheric conditions, *J. Atmos. Sci.*, *57*, 3752-3766.

DeMott, P. J., D. J. Cziczo, A. J. Prenni, D. M. Murphy, S. M. Kreidenweis, D. S. Thompson, R. Borys, and D. C. Rogers (2003), Measurements of the concentration and composition of nuclei for cirrus formation, *Proc. Natl. Acad. Sci. USA*, *100*, 14655-14660.

DeMott, P. J., M. P. Meyers, and R. W. Cotton (1994), Parameterization and impact of ice initiation processes relevant to numerical model simulations of cirrus clouds, *J. Atmos. Sci.*, *51*, 77-90.

DeMott, P. J., D. C. Rogers, and S. M. Kreidenweis (1997), The susceptibility of ice formation in upper tropospheric clouds to insoluble aerosol components, *J. Geophys. Res.*, *102*, 19575-19584.

DeMott, P. J., D. C. Rogers, S. M. Kreidenweis, Y. Chen, C. H. Twohy, D. G. Baumgardner, A. J. Heymsfield, and K. R. Chan (1998), The role of heterogeneous freezing nucleation in upper tropospheric clouds: inferences from SUCCESS, *Geophys. Res. Lett.*, *25*, 1387-1390.

Fountoukis, C., and A. Nenes (2005), Continued development of a cloud droplet formation parameterization for global climate models, *J. Geophys. Res.*, *110*, D11212, doi:11210.11029/12004JD005591.

Fridlind, A. M., A. S. Ackerman, E. J. Jensen, A. J. Heymsfield, M. R. Poellot, D. E. Stevens, D. Wang, L. M. Miloshevich, D. G. Baumgardner, P. Lawson, J. Willson, R. C. Flagan, J. H. Seinfeld, H. H. Jonsson, T. M. VanReken, V. Varutbangkul, and T. A. Rissman (2004), Evidence for the predominance of mid-tropospheric aerosols as subtropical anvil cloud nuclei, *Science*, *304*, 718-722.

Gayet, J. F., J. Ovarlez, V. Shcherbakov, J. Ström, U. Schumann, A. Minikin, F. Auriol, A. Petzold, and M. Monier (2004), Cirrus cloud microphysical and optical properties at southern and northern midlatitudes during the INCA experiment, *J. Geophys. Res.*, *109*, D20206.

Gelbard, F., and J. H. Seinfeld (1980), Simulation of multicomponent aerosol dynamics, *Journal of Colloid and Interface Science*, *78*, 485-501.

Gershenzon, M., P. Davidovits, L. R. Williams, Q. Shin, J. T. Jayne, C. H. Kolb, and D. R. Worsnop (2004), Uptake of $H_2{}^{17}O(g)$ and $D_2O(q)$ by aqueous sulfuric acid droplets, *J. Phys. Chem. A*, *108*, 1567-1573.

Gierens, K. (2003), On the transition between heterogeneous and homogeneous freezing *Atmos. Chem. Phys.*, *3*, 437-446.

Gierens, K., M. Monier, and J. F. Gayet (2003), The deposition coefficient and its role for cirrus clouds, *J. Geophys. Res.*, *108*, 4069.

Haag, W., B. Kärcher, S. Schaefers, O. Stetzer, O. Möhler, U. Schurath, M. Krämer, and C. Schiller (2003a), Numerical simulations of homogeneous freezing processes in the aerosol chamber AIDA, *Atmos. Chem. Phys.*, *3*, 195-210.

Haag, W., B. Kärcher, J. Strom, A. Minikin, U. Lohmann, J. Ovarlez, and A. Stohl (2003b), Freezing thresholds and cirrus formation mechanisms inferred from in situ measurements of relative humidity, *Atmos. Chem. Phys.*, *3*, 1791-1806.

Hartmann, D. L., J. R. Holton, and Q. Fu (2001), The heat balance of the tropical tropopause, cirrus, and stratospheric dehydration *Geophys. Res. Lett.*, *28*, 1969-1972.

Haynes, D. R., N. J. Tro, and S. M. George (1992), Condensation and evaporation of H_2O on ice surfaces, *J. Phys. Chem.*, *96*, 8502-8509.

Heymsfield, A. J., and L. M. Miloshevich (1995), Relative humidity and temperature influences on cirrus formation and evolution: observations from wave clouds and FIRE II, *J. Atmos. Sci.*, *52*, 4302.

Heymsfield, A. J., and R. M. Sabin (1989), Cirrus crystal nucleation by homogenous freezing of solution droplets., *J. Atmos. Sci.*, *46*, 2252.

Hoyle, C. R., B. P. Luo, and T. Peter (2005), The origin of high ice crystal number densities in cirrus clouds, *J. Atmos. Sci.*, *62*, 2658-2579.

IPCC (2007), *Climate change 2007: the physical basis. Contribution of working group I to the fourth assessment report of the Intergovernmental Panel on Climate*

Change. , Cambridge University Press, Cambridge, United Kingdom and New York, NY, USA.

Jensen, E. J., and O. B. Toon (1994), Ice nucleation in the upper troposphere: sensitivity to aerosol number density, temperature, and cooling rate, *Geophys. Res. Lett.*, *21*, 2019-2022.

Jensen, E. J., O. B. Toon, D. L. Westphal, S. Kinne, and A. J. Heymsfield (1994), Microphysical modeling of cirrus 1. Comparison with 1986 FIRE IFO measurements, *J. Geophys. Res.*, *99*, 10421-10442.

Kärcher, B., J. Hendricks, and U. Lohmann (2006), Physically based parameterization of cirrus cloud formation for use in global atmospheric models, *J. Geophys. Res.*, *111*, D01205.

Kärcher, B., and T. Koop (2005), The role of organic aerosols in homogeneous ice formation, *Atmos. Chem. Phys.*, *5*, 703-714.

Kärcher, B., and U. Lohmann (2002a), A parameterization of cirrus cloud formation: homogeneous freezing including effects or aerosol size, *J. Geophys. Res.*, *107*, 4698, doi:4610.1029/2001JD001429.

Kärcher, B., and U. Lohmann (2002b), A parameterization of cirrus cloud formation: homogeneous freezing of supercooled aerosols, *J. Geophys. Res.*, *107*, 4010, doi:4010.1029/2001JD000470.

Kärcher, B., and U. Lohmann (2003), A parameterization of cirrus cloud formation: Heterogeneous freezing *J. Geophys. Res.*, *108*, 4402, doi:4410.1029/2002JD003220.

Kärcher, B., and J. Ström (2003), The roles of dynamical variabilty and aerosols in cirrus cloud formation, *Atmos. Chem. Phys.*, *3*, 823-838.

Khvorostyanov, V. I., and J. A. Curry (2005), The theory of ice nucleation by heterogeneous freezing of deliquescent mixed CCN. Part II: parcel model simulations, *J. Atmos. Sci.*, *62*, 261-285.

Khvorostyanov, V. I., H. Morrison, J. A. Curry, D. G. Baumgardner, and P. Lawson (2006), High supersaturation and modes of ice nucleation in thin tropopause cirrus: simulation of the 13 July 2002 cirrus regional study of tropical anvils and cirrus layers case, *J. Geophys. Res.*, *111*, D02201, doi:02210.01029/02004JD005235.

Koenig, R. L. (1972), Parameterization of ice growth for numerical calculations of cloud dynamics, *Mon. Weather Rev.*, *100*, 417-423.

Koop, T., B. Luo, A. Tslas, and T. Peter (2000), Water activity as the determinant for homogeneous ice nucleation in aqueous solutions, *Nature*, *406*, 611-614.

Lin, H., K. J. Noone, J. Ström, and A. J. Heymsfield (1998), Dynamical influences on cirrus cloud formation process, *J. Atmos. Sci.*, *55*, 1940-1943.

Lin, R., D. Starr, P. J. DeMott, R. Cotton, K. Sassen, E. J. Jensen, B. Kärcher, and X. Liu (2002), Cirrus parcel model comparison project. Phase 1: The critical components to simulate cirrus initiation explicitly., *J. Atmos. Sci.*, *59*, 2305-2328.

Liou, K. (1986), Influence of cirrus clouds on weather and climate processes: a global perspective, *Mon. Weather Rev.*, *114*, 1167-1199.

Liu, X., and J. E. Penner (2005), Ice nucleation parameterization for global models, *Meteorol. Z.*, *14*, 499-514.

Liu, X., J. E. Penner, S. J. Ghan, and M. Wang (2007), Inclusion of ice mycrophysics in the NCAR Community Atmospheric Model version 3 (CAM3), *J. Clim.*, *20*, 4526-4547.

Lohmann, U., and B. Kärcher (2002), First interactive simulations of cirrus clouds formed by homogeneous freezing in the ECHAM general circulation model *J. Geophys. Res.*, *107*, 4105, doi:4110.1029/2001JD000767.

Minnis, P. (2004), Contrails, cirrus trend, and climate, *J. Clim.*, *17*, 1671-1685.

Möhler, O., O. Stetzer, C. Linke, M. Schnaiter, R. Tiede, H. Saathoff, M. Krämer, A. Mangold, P. Budz, P. Zink, J. Schreiner, K. Mauersberger, W. Haag, B. Kärcher, and U. Schurath (2003), Experimental investigation of homogeneous freezing of sulfuric acid particles in the aerosol chamber AIDA, *Atmos. Chem. Phys.*, *3*, 211-223.

Monier, M., W. Wobrock, J. F. Gayet, and A. Flossman (2006), Development of a detailed microphysics cirrus model tracking aerosol particles. Histories for interpretation of the recent INCA campaign, *J. Atmos. Sci.*, *63*, 504-525.

Murphy, D. M., and T. Koop (2005), Review of the vapour pressures of ice and supercooled water for atmospheric applications, *Q. J. R. Meteorol. Soc.*, *131*, 1539-1565.

Myhre, C. E., C. J. Nielsen, and O. E. Saastad (1998), Density and surface tension of aqueous H_2SO_4 at low temperatures *J.Chem. Eng. Data*, *43*, 617-622.

Penner, J. E., D. H. Lister, D. J. Griggs, D. J. Dokken, and M. McFarland (1999), *Aviation and the global atmosphere - A special report of IPCC working groups I*

and III. Intergovernmental Panel on Climate Change., 365 pp., Cambridge University Press.

Pruppacher, H. R., and J. D. Klett (1997), *Microphysics of clouds and precipitation* 2nd ed., Kluwer Academic Publishers, Boston, MA

Ramanathan, V., and W. Collins (1991), Thermodynamic regulation of ocean warming by cirrus clouds deduced from observations of 1987 El Nino, *Nature*, *351*, 27-32.

Ren, C., and A. R. Mackenzie (2005), Cirrus parameterization and the role of ice nuclei, *Q. J. R. Meteorol. Soc.*, *131*, 1585-1605.

Sassen, K., and S. Benson (2000), Ice nucleation in cirrus clouds: a model study of the homogeneous and heterogeneous modes, *Geophys. Res. Lett.*, *27*, 521-524.

Seifert, M., J. Strom, R. Krejci, A. Minikin, A. Petzold, J.-F. Gayet, H. Schlager, H. Ziereis, U. Schumann, and J. Ovarlez (2004), Aerosol-cirrus interactions: a number based phenomenon at all?, *Atmos. Chem. Phys.*, *4*, 293-305.

Seinfeld, J. H., and S. N. Pandis (1998), *Atmospheric Chemistry and Physics*, John Wiley and Sons, New York, NY, USA.

Stuber, N., P. Forster, G. Radel, and K. Shine (2006), The importance of the diurnal and annual cycle of air traffic for contrail radiative forcing, *Nature*, *441*, 864-867.

Tabazadeh, A., and E. J. Jensen (1997), A model description for cirrus nucleation from homogeneous freezing of sulfate aerosols *J. Geophys. Res.*, *102*, 23845-23850.

Tabazadeh, A., O. B. Toon, and E. J. Jensen (1997), Formation and implications of ice particle nucleation in the stratosphere, *Geophys. Res. Lett.*, *24*, 2007-2010.

Twomey, S. (1959), The nuclei of natural cloud formation. II. The supersaturation in natural clouds and the variation of cloud droplet number concentration, *Pure Appl. Geophys.*, *43*, 243-249, doi:210.1007/BF01993560.

Wood, S. E., M. B. Baker, and D. Calhoun (2001), New model for the vapor growth of hexagonal ice crystals in the atmosphere, *J. Geophys. Res.*, *106*, 4845-4870.

Table 1. Cloud formation conditions used in evaluation.

Property	Values
T (K)	200-235
V (m s^{-1})	0.02-5
α_d	0.05-1.0
$\sigma_{g,\,dry}$	1.7, 2.3, 2.9
N_o (cm^{-3})	10-5000
$D_{g,\,dry}$ (nm)	20-160

Figure Captions

Figure 1. Lagrangian particle-tracking scheme for a hypothetical population of two liquid droplets during three successive time steps. Circles represent supercooled liquid droplets, and hexagons ice crystals. Black arrows indicate growth and aging whereas red arrows onset of freezing. Transition of light to darker shady indicates temporal evolution.

Figure 2. Sketch of the parameterization concept. Circles represent supercooled liquid droplets, and hexagons ice crystals.

Figure 3. S_i, N_c, and ice water content (IWC) profiles obtained from the numerical solution of the parcel model. Cases considered are those of *Lin et al.* [2002]. Solid lines indicates T_o = 233 K and dashed lines T_o = 213 K. V=0.04 m s^{-1} (upper), 0.2 m s^{-1} (middle), and 1 m s^{-1} (lower).

Figure 4. Parameterization algorithm.

Figure 5. S_i (red, left axes) and N_c (blue, right axes) evolution calculated by the parcel model. T and V conditions shown are 233 K and 1 m s^{-1} (top right), 203 K and 1 m s^{-1} (top left), 233 K and 0.04 m s^{-1} (bottom right), 203 K and 0.04 m s^{-1} (bottom left). Dashed lines represent the time at which $S_{i,max}$ is reached and dotted lines S_i evolution under "free growth".

Figure 6. Crystal size distribution calculated by the parcel model and the parameterization at $S_{i,max}$. Left, T=213 K V= 1.0 m s^{-1}. Right, T=233 K V= 0.2 m s^{-1}. $\sigma_{g,\,dry}$ is the geometric dispersion of the aerosol size distribution.

Figure 7. Ice crystal number concentration calculated by the parcel model and the parameterization. $D_{c,s_{\max}}$ was calculated using either equation (31) (right) or (32) (left).

Gray scale represents the value of α_d used in the calculations; dashed lines represent the ± 50 % difference.

Figure 8. Ice crystal number concentration as a function of the updraft velocity, calculated using the parcel model (symbols), KL2002 (dashed line), LP2005 (dashed-dotted line), SB2000 (dotted line), and the theoretical (stars), and adjusted (solid line) parameterizations. Results are shown for T=233 K, p=34000 Pa (right) and T = 213 K, p=17000 Pa (left), and α_d = 0.1 (black) and α_d = 1.0 (blue). N_o=200 cm^{-3}, and $D_{g,dry}$ = 40 nm.

Figure 9. Ice crystal number concentration as a function of the aerosol number concentration. Symbols as in Figure 8. Results are shown for V= 0.2 m s^{-1} (left) and 1 m s^{-1}, and T=233 K, p=38812 Pa (blue) and T = 213 K, p=27350 Pa (black). α_d = 0.1, and $D_{g,dry}$ = 40 nm.

Figure 10. Ice crystal number concentration as a function of the aerosol mean dry diameter. Symbols as in Figure 8. Results are shown for T=233 K, p=34000 Pa (right) and T = 213 K, p=17000 Pa (left), and α_d = 0.1 (black) and α_d = 1.0 (blue). N_o=200 cm^{-3}, and V= 1 m s^{-1}.

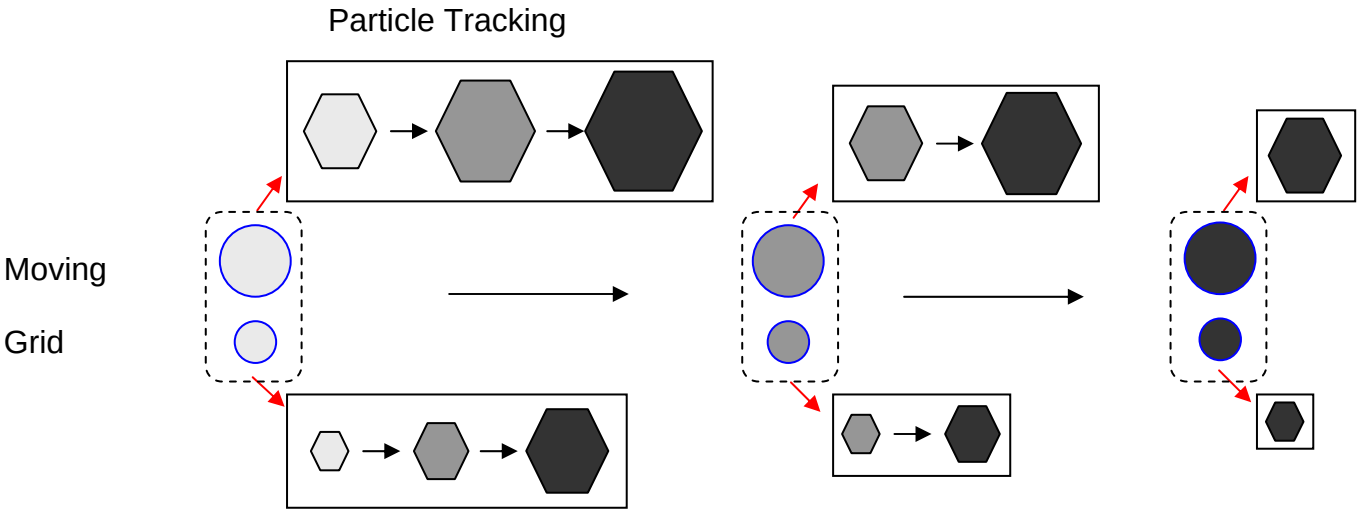

FIGURE 1

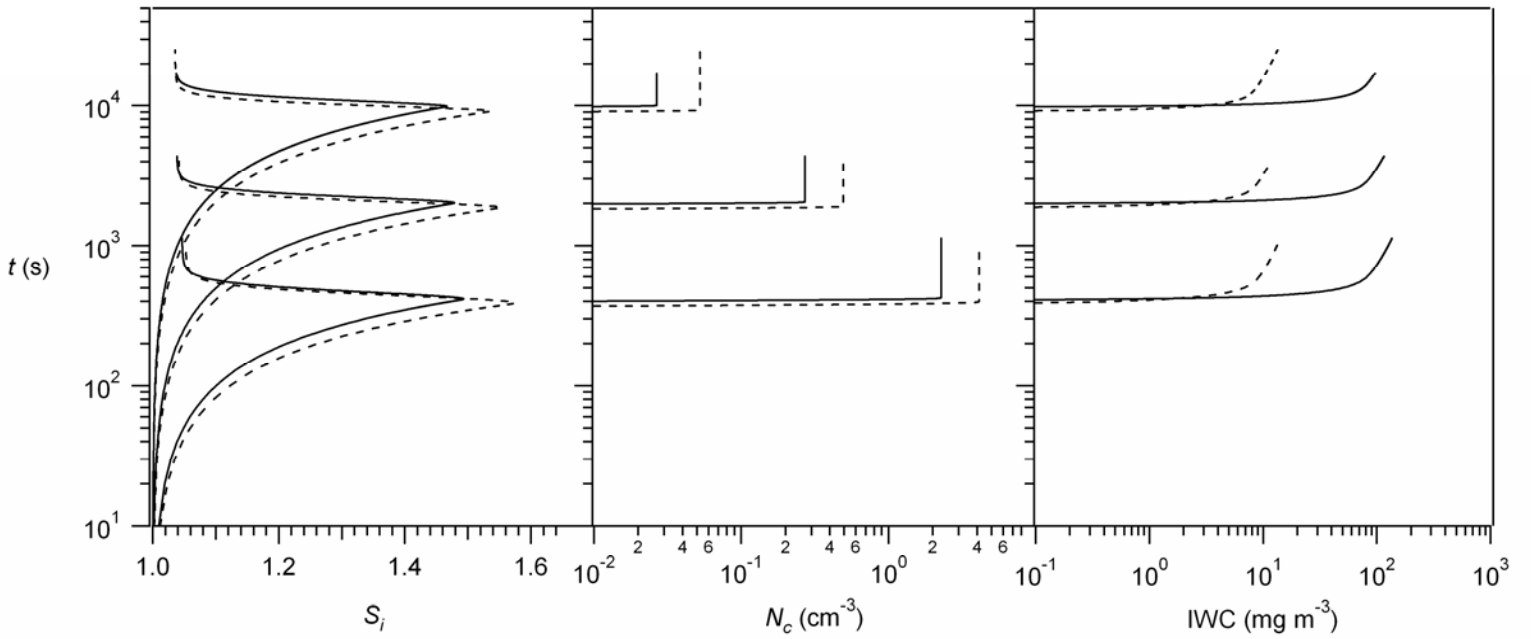
t (s)
10^4
10^3
10^2
10^1
1.0
1.2
1.4
1.6
S_i
10^-2
2
4
6
10^-1
2
4
6
10^0
2
4
6
N_c (cm^-3)
10^-1
10^0
10^1
10^2
10^3
IWC (mg m^-3)

FIGURE 2

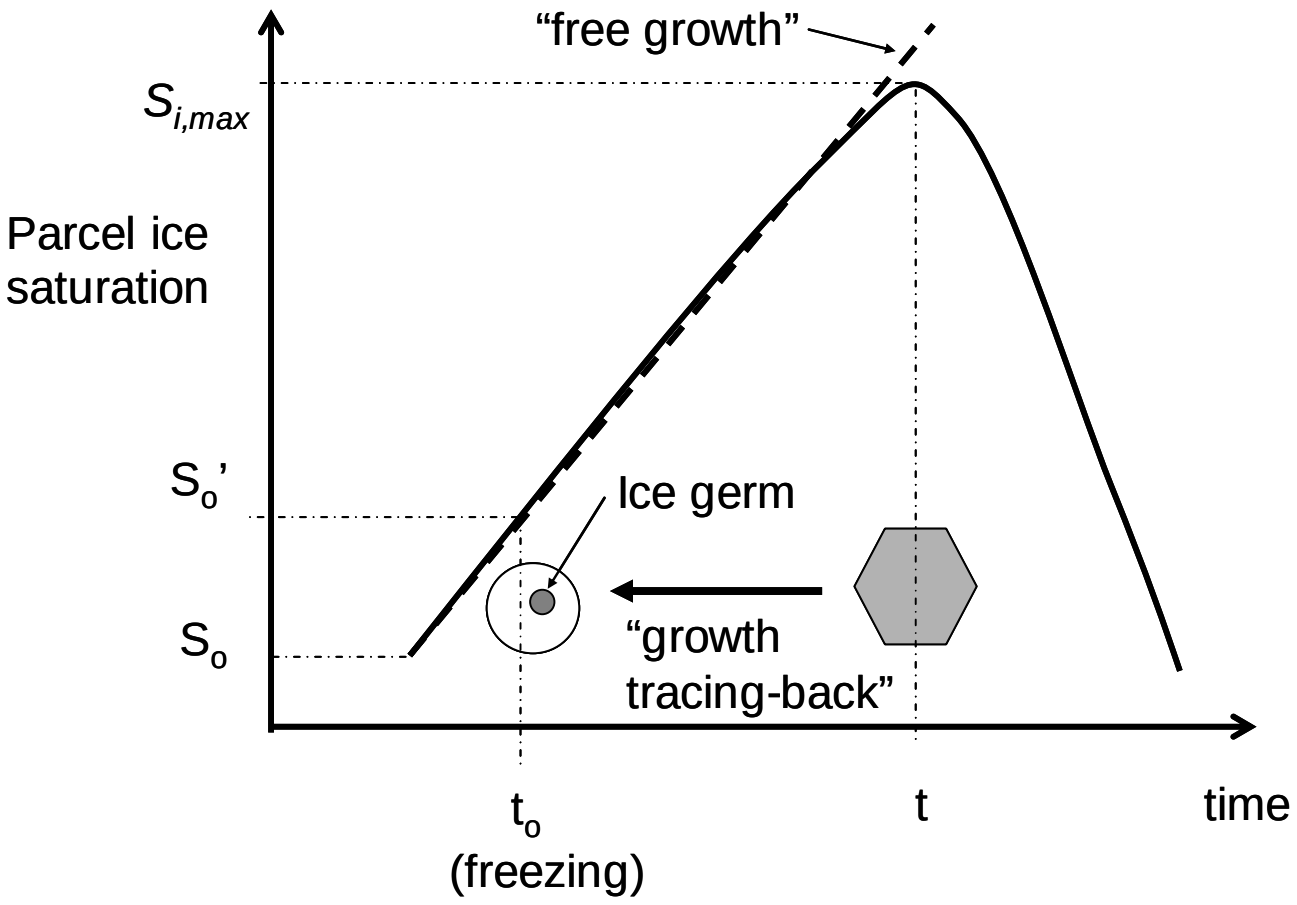
"free growth"
$S_{i,max}$
Parcel ice saturation
S_o'
Ice germ
S_o
"growth tracing-back"
t_o
(freezing)
t
time

FIGURE 3

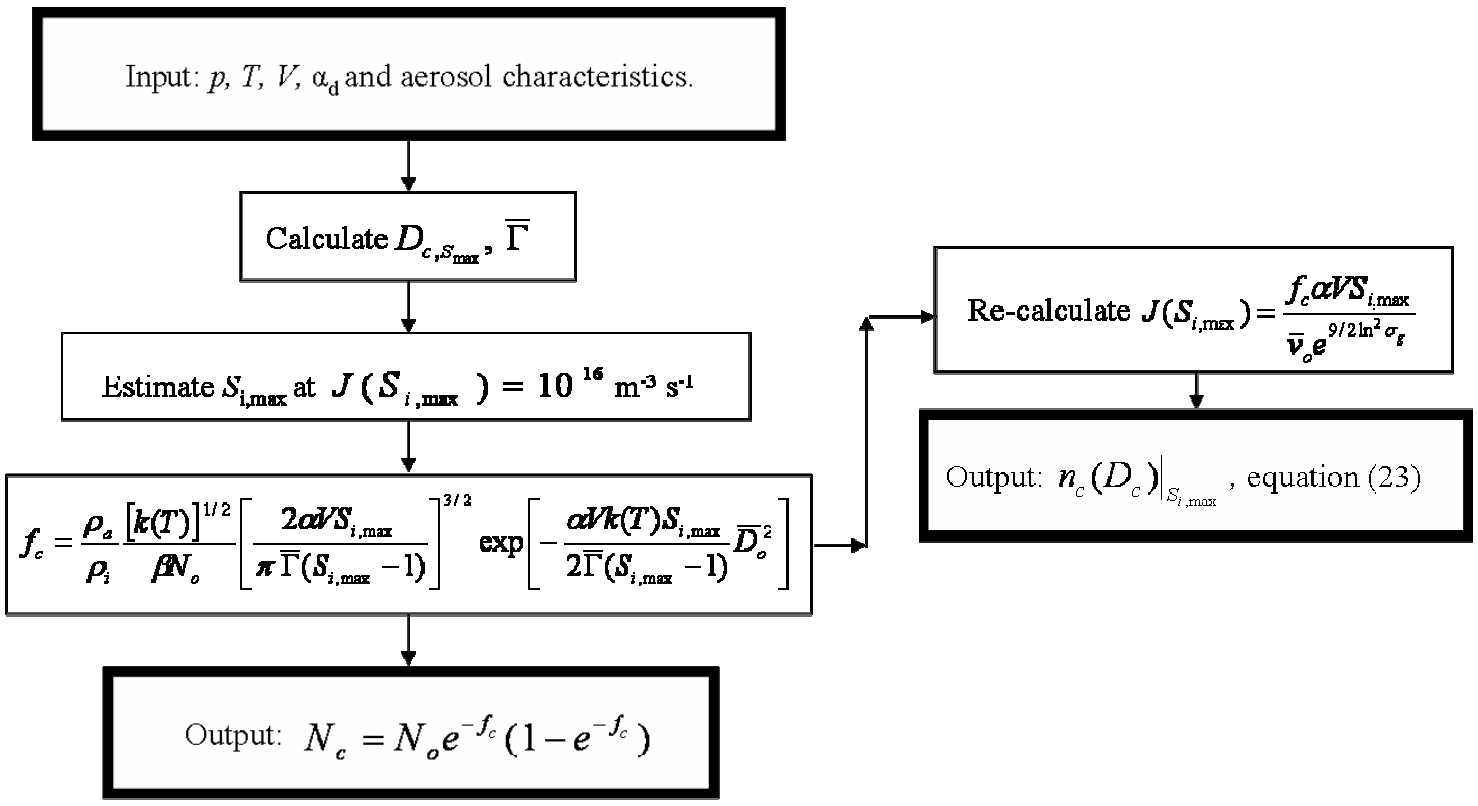
Input: p, T, V, α_d and aerosol characteristics.
Calculate $D_{c,S_{max}}$, $\overline{\Gamma}$
Estimate $S_{i,max}$ at $J(S_{i,max}) = 10^{16}$ m^{-3} s^{-1}
$f_c = \frac{\rho_a}{\rho_i}\frac{[k(T)]^{1/2}}{\beta N_o}\left[\frac{2\alpha V S_{i,max}}{\pi\overline{\Gamma}(S_{i,max}-1)}\right]^{3/2}\exp\left[-\frac{\alpha V k(T) S_{i,max}}{2\overline{\Gamma}(S_{i,max}-1)}\overline{D}_o^2\right]$
Output: $N_c = N_o e^{-f_c}(1-e^{-f_c})$
Re-calculate $J(S_{i,max}) = \frac{f_c \alpha V S_{i,max}}{\overline{\nu}_o e^{9/2\ln^2\sigma_g}}$
Output: $n_c(D_c)|_{S_{i,max}}$, equation (23)

FIGURE 4

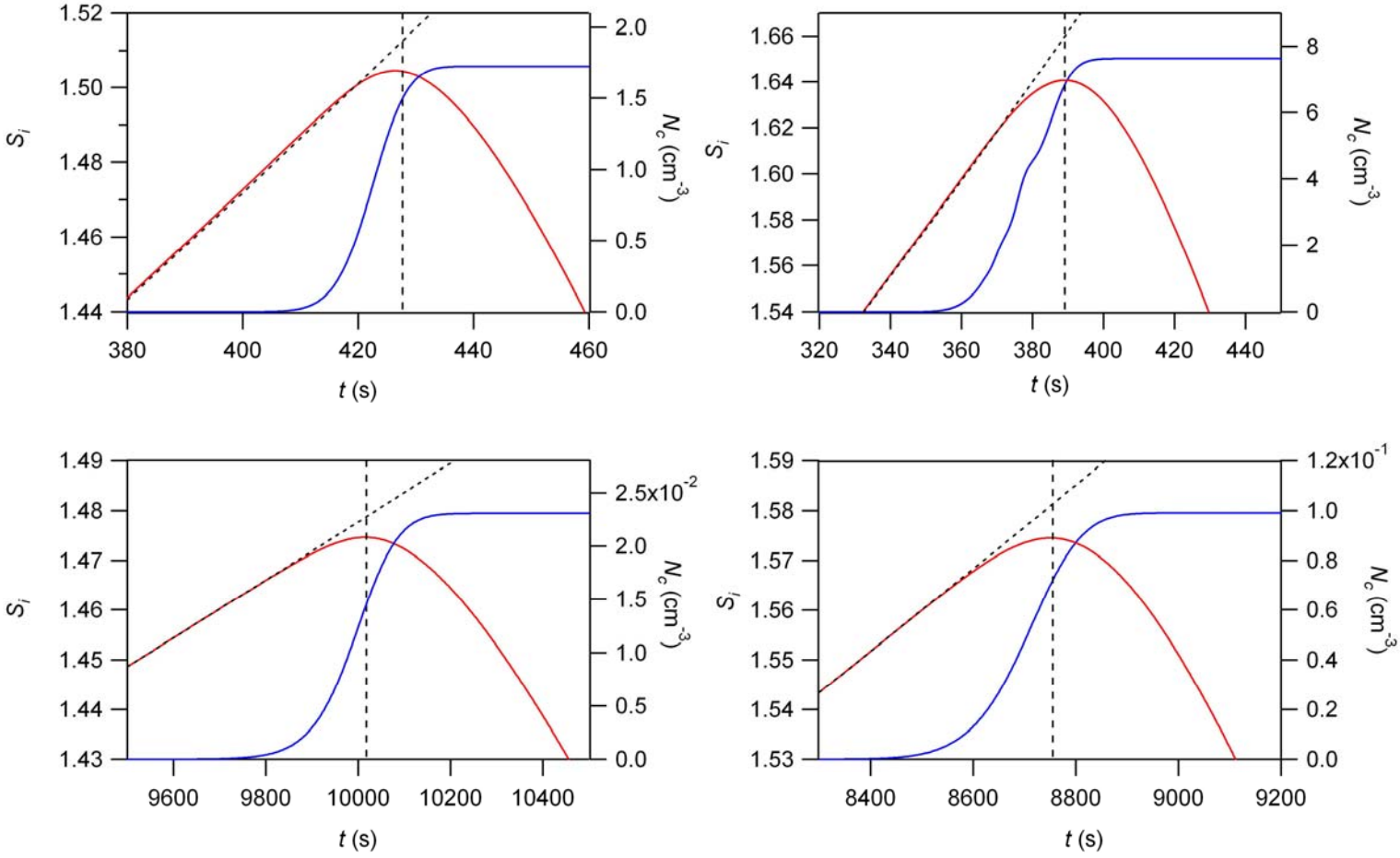
1.52
1.50
1.48
1.46
1.44
S_i
2.0
1.5
1.0
0.5
0.0
N_c (cm^{-3})
380
400
420
440
460
t (s)
1.66
1.64
1.62
1.60
1.58
1.56
1.54
S_i
8
6
4
2
0
N_c (cm^{-3})
320
340
360
380
400
420
440
t (s)
1.49
1.48
1.47
1.46
1.45
1.44
1.43
S_i
2.5x10^{-2}
2.0
1.5
1.0
0.5
0.0
N_c (cm^{-3})
9600
9800
10000
10200
10400
t (s)
1.59
1.58
1.57
1.56
1.55
1.54
1.53
S_i
1.2x10^{-1}
1.0
0.8
0.6
0.4
0.2
0.0
N_c (cm^{-3})
8400
8600
8800
9000
9200
t (s)

FIGURE 5

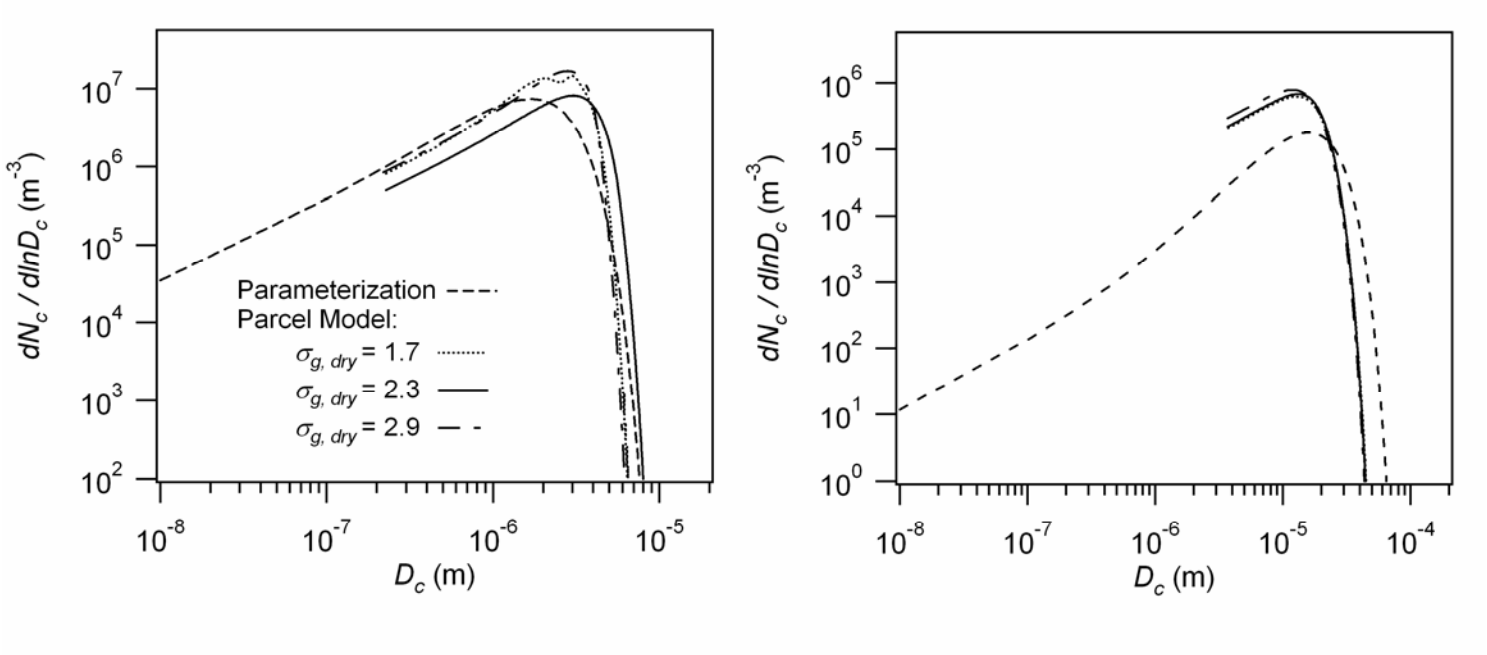
$dN_c / dlnD_c$ (m^{-3})
D_c (m)
Parameterization
Parcel Model:
$\sigma_{g,\,dry}$ = 1.7
$\sigma_{g,\,dry}$ = 2.3
$\sigma_{g,\,dry}$ = 2.9

FIGURE 6

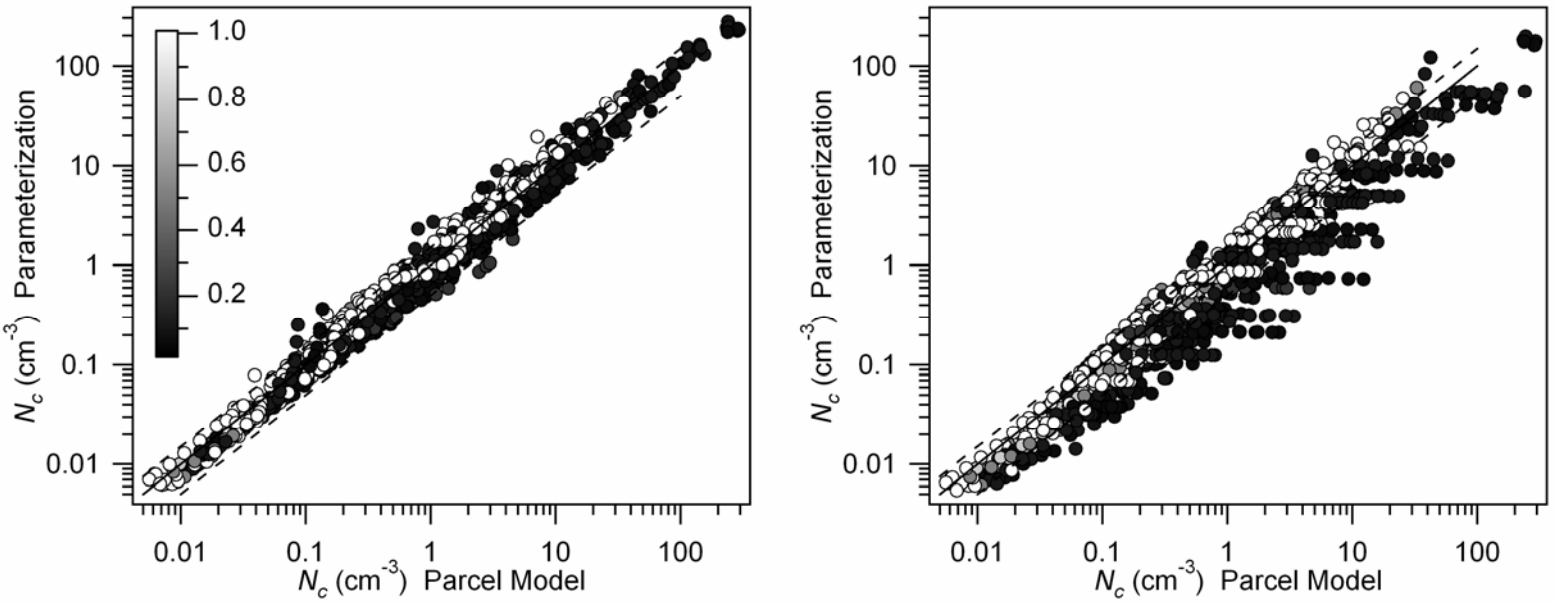
1.0
0.8
0.6
0.4
0.2
100
10
1
0.1
0.01
N_c (cm^{-3}) Parameterization
0.01
0.1
1
10
100
N_c (cm^{-3}) Parcel Model
100
10
1
0.1
0.01
N_c (cm^{-3}) Parameterization
0.01
0.1
1
10
100
N_c (cm^{-3}) Parcel Model

FIGURE 7

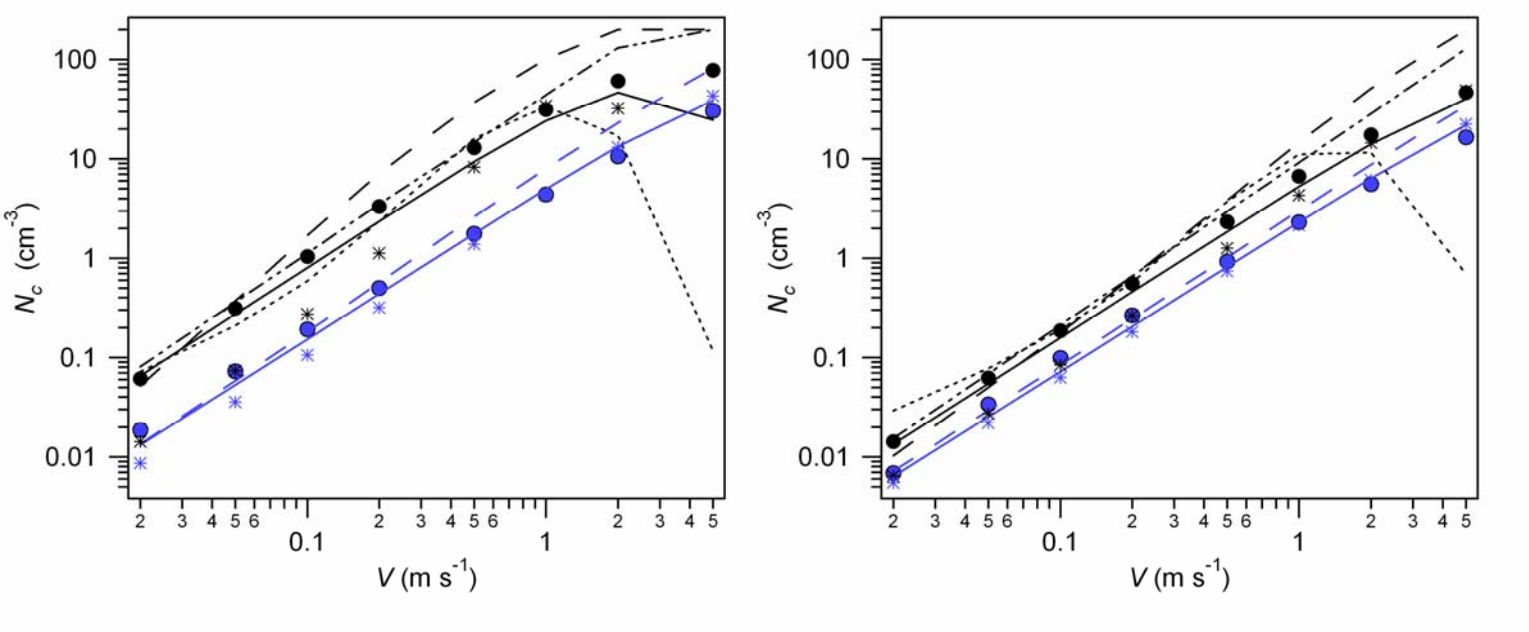
100
10
1
0.1
0.01
N_c (cm^{-3})
2 3 4 5 6 0.1 2 3 4 5 6 1 2 3 4 5
V (m s^{-1})
100
10
1
0.1
0.01
N_c (cm^{-3})
2 3 4 5 6 0.1 2 3 4 5 6 1 2 3 4 5
V (m s^{-1})

FIGURE 8

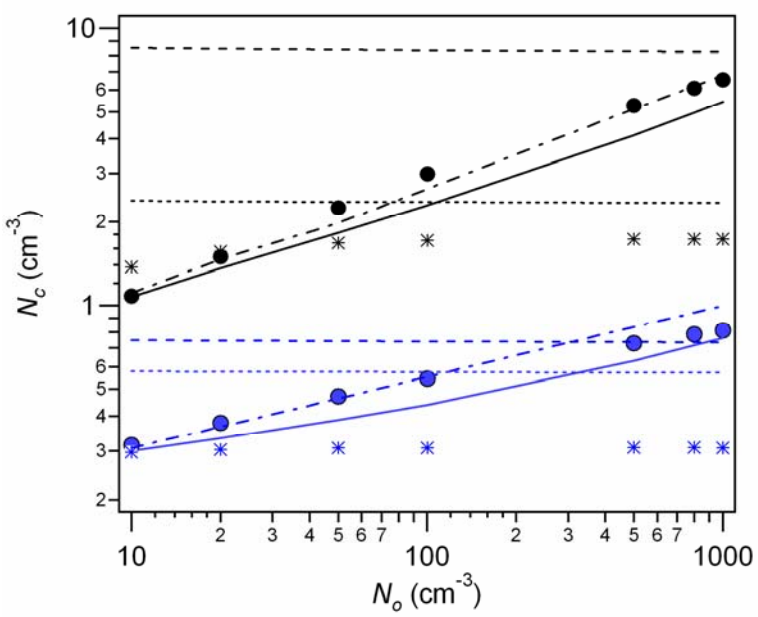
10
6
5
4
3
2
1
6
5
4
3
2
N_c (cm^{-3})
10
2
3
4
5
6
7
100
2
3
4
5
6
7
1000
N_o (cm^{-3})

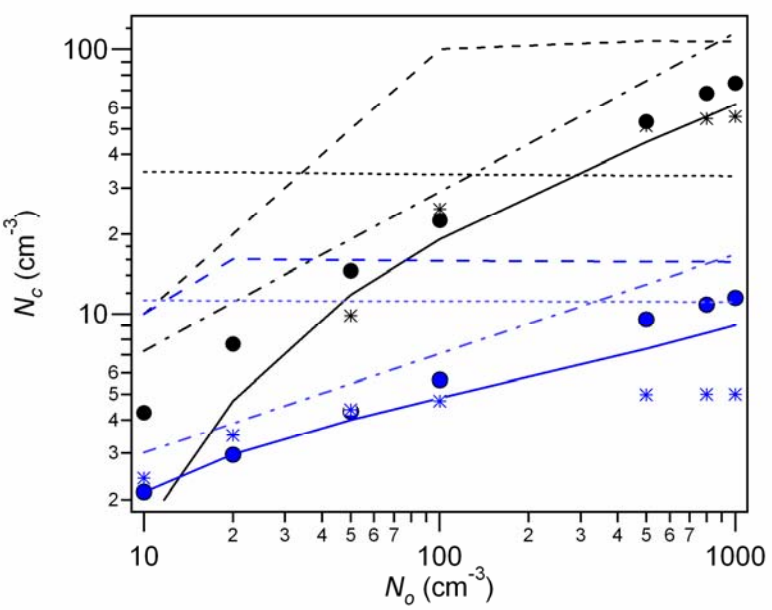
100
6
5
4
3
2
10
6
5
4
3
2
N_c (cm^{-3})
10
2
3
4
5
6
7
100
2
3
4
5
6
7
1000
N_o (cm^{-3})

FIGURE 9

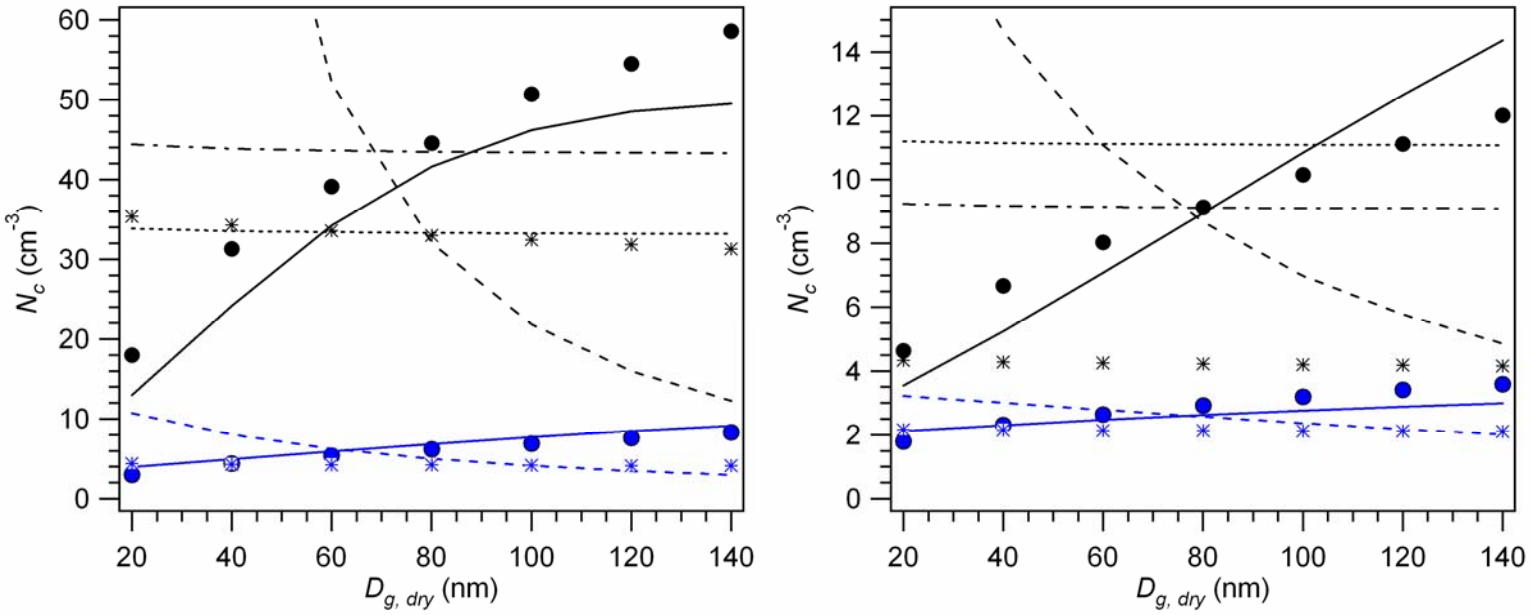
N_c (cm^{-3})
$D_{g,\ dry}$ (nm)
0
10
20
30
40
50
60
20
40
60
80
100
120
140
N_c (cm^{-3})
$D_{g,\ dry}$ (nm)
0
2
4
6
8
10
12
14
20
40
60
80
100
120
140

FIGURE 10